# GEDI Launches a New Era of Biomass Inference from Space

# GEDI Launches a New Era of Biomass Inference from Space

Ralph Dubayah[1*], John Armston[1], Sean P. Healey[2], Jamis M Bruening[1], Paul L. Patterson[2], James R. Kellner[3], Laura Duncanson[1], Svetlana Saarela[4], Göran Ståhl[5,] Zhiqiang Yang[2], Hao Tang[1,6], J. Bryan Blair[7], Lola Fatoyinbo[7], Scott Goetz[8], Steven Hancock[9], Matt Hansen[1], Michelle Hofton[1], George Hurtt[1], Scott Luthcke[7]

---

*email: dubayah@umd.edu

[1]Department of Geographical Sciences, University of Maryland, College Park, MD USA

[2]USDA Forest Service Rocky Mountain Research Station, Ogden, UT USA

[3]Department of Ecology, Evolution and Organismal Biology, Brown University, Providence, RI USA

[4]Faculty of Environmental Sciences and Natural Resource Management, Norwegian University of Life Sciences, Ås, Norway

[5]Department of Forest Resource Management, Swedish University of Agricultural Sciences, Umeå, Sweden.

[6]Department of Geography, National University of Singapore, Singapore

[7]NASA Goddard Space Flight Center, Greenbelt, MD, USA

[8]Northern Arizona University, Flagstaff, AZ, USA

[9]School of Geosciences, The University of Edinburgh, Edinburgh, United Kingdom

## Abstract

Accurate estimation of aboveground forest biomass stocks is required to assess the impacts of land use changes such as deforestation and subsequent regrowth on concentrations of atmospheric $CO_2$. The Global Ecosystem Dynamics Investigation (GEDI) is a lidar mission launched by NASA to the International Space Station in 2018. GEDI was specifically designed to retrieve vegetation structure within a novel, theoretical sampling design that explicitly quantifies biomass and its uncertainty across a variety of spatial scales. In this paper we provide the estimates of pan-tropical and temperate biomass derived from two years of GEDI observations. We present estimates of mean biomass densities at 1 km resolution, as well as estimates aggregated to the national level for every country GEDI observes, and at the sub-national level for the United States. For all estimates we provide the standard error of the mean biomass. These data serve as a baseline for current biomass stocks and their future changes, and the mission's integrated use of formal statistical inference points the way towards the possibility of a new generation of powerful monitoring tools from space.

# Introduction

The place of formalized inference has long been recognized in applications such as opinion polling and product quality control, where measurement of every individual is impossible and there must be a means of understanding the likelihood that one's sample is representative. Ground-based forest inventories have been organized around probabilistic sampling for well over 100 years (*1*). While the use of satellite remote sensing for forest inventory has grown considerably, methods have been slow to embrace formal estimation using remote sensing, in part because values predicted for variables such as biomass using wall-to-wall imagery may simply be summed or averaged over large areas without appealing to sampling theory. However, remote sensing scientists have begun to realize that a theoretical framework is needed to address the potential impact of modeling error in these maps when they are used to describe ecosystem properties, particularly when the remote sensing data themselves are samples, that is, are not spatially continuous (*2, 3*).

Forest biomass stocks are one of the major uncertainties in the global carbon cycle and their local-scale estimation is a prime challenge using remote sensing. Our ability to infer the impact of land use changes such as deforestation and reforestation on concentrations of atmospheric $CO_2$ rests upon accurate and spatially resolved estimates of aboveground biomass (AGB) and density (AGBD) (*4, 5*). Maps of localized biomass estimates, when combined with spatial records of recent land use change (*6, 7*), support policy-critical decisions about the role of ecosystem dynamics in the climate system. Additionally, having an accurate representation of biomass is essential for the initialization of prognostic ecosystem models used to explore carbon sequestration potential of forests under changing land use and climate change scenarios (*8*).

Aircraft-mounted laser-based lidar instruments have collected high-quality forest biomass measurements in local- to national-scale projects around the world (*9, 10*), and space-based lidar

data from ICESat GLAS (the Geoscience Laser Altimeter System) have figured centrally in many of the most prominent existing global-scale biomass maps (*11–13*). However, GLAS was not engineered for forest monitoring, and coverage of forests conformed to no identifiable sample design – often covering the same orbital paths dozens of times and leaving large areas unmeasured. Efforts to use GLAS have fallen into three general categories, each limited in a specific way. Some efforts have knowingly treated GLAS overpasses as if they were randomly allocated, allowing use of analytically grounded hybrid model-based methods of variance estimation but potentially underestimating variance due to the discrepancy between the hypothetical and actual sample designs (*14*, *15*). One study alternatively subset available GLAS data to what could be presumed to be a spatially balanced random sample, but suffered a substantial drop in statistical power because of the large quantity of data that was eliminated (*16*). Lastly, some efforts have treated biomass predictions at GLAS footprints as pseudo-plots used to train a second level of model based upon passive optical reflectance data. Lack of an analytical framework linking uncertainties from multiple models and GLAS' sampling process generally necessitated *ad hoc* error propagation in these efforts, which sometimes produced significantly different estimates over the same areas (*17*).

In response to the continuing need for accurate observation of canopy structure within an inferential sampling framework designed for biomass estimation across scales, the Global Ecosystem Dynamics Investigation (GEDI) was developed by NASA (*18*). GEDI uses a multi-beam lidar (Fig. S1) to provide 8 transects of canopy vertical structure at 25 m footprint resolution. Launched to the International Space Station in late 2018, GEDI is specifically optimized to estimate biomass through direct measurement of canopy structure. GEDI's design supports analytical, closed-form estimation of AGBD in several ways. First, the spatial dimensions of the footprints over which GEDI measures canopy height distribution approximately match both the areas of conventional field plots and the pixel size of medium-

resolution sensors that may be used to model GEDI height metrics across continuous surfaces. Models linking lidar observables to both field measurements and biomass map units can suffer from dilution of precision when there are discrepancies in the amount of ground area covered or if there are significant geolocation errors between lidar metrics and plots (*19*). GEDI avoids the latter by using a pre-launch calibration strategy based on simulated lidar metrics from precisely located airborne lidar data. Secondly, GEDI predictions of biomass for every footprint are calibrated with the most extensive global set of coincident field and aircraft data yet compiled. Closed-form model-based statistical estimators conventionally accommodate only linear parametric models (*3*) (though see Esteban et al. (*20*)) and GEDI's footprint biomass estimation process was created to use such models. The consequence of these first two design strategies is that they enable closed-form estimators for AGBD. GEDI's 25 m footprint biomass predictions are used with hybrid model-based estimators (*21*) to infer biomass within each 1 km grid cell across the mission's range of observation. The parametric models mentioned above are used to predict biomass for all footprints within a given grid cell, and the hybrid estimates of variance of the mean account for both modeling uncertainty and uncertainty related to how the cell is sampled by GEDI's observations (*18*). Furthermore, hybrid inference directly enables robust estimates at any aggregation scale coarser than 1 km (e.g., a country) without resorting to the *ad hoc* and approximate methods used in other remote sensing biomass products.

Here, we report the 1 km estimates of biomass from this integrated mission. Current estimates use more than 5 billion footprint-level biomass predictions collected by GEDI across 2.5 years of observations beginning in April 2019. GEDI's frame of inference can also be focused upon broader scales, and we present additional estimates at: (1) the scale of individual countries observed by GEDI, and (2) at the scale of ~12,000, 640 $km^2$ hexagons covering the conterminous United States. We compare these estimates to available reference data by way of validation. We further describe the unplanned orbital resonance that affected the ISS after GEDI's first year on

orbit and detail how the mission's sample design accommodated this development. These new GEDI data provide a much-needed baseline for biomass stocks of tropical and temperate regions for the current epoch and serve as a foundational data set for higher resolution mapping using remote sensing fusion methods.

## Methods

**GEDI-based biomass estimation at the 1 km, hexagon, and country levels**

Aboveground biomass density was estimated for every footprint that measured valid height metrics along each of GEDI's 8 tracks (see Supplementary Materials: Footprint-Level Biomass Estimation). All estimates presented here were produced through the same inferential process: (1) high-quality GEDI waveforms falling within an area of interest were treated as a randomly allocated cluster sample oriented around laser ground tracks; (2) aboveground biomass density was predicted for the footprint of each waveform using a parametric model derived from a global set of calibration data; (3) mean AGBD and uncertainty of that mean for the area of interest were estimated using hybrid model-based estimators (*21*).

Waveforms comprising the sample were collected from 18th April 2019 to 4th August 2021 and the following criteria were used to identify high-quality shots.

1. Shots flagged as quality by the GEDI L2A Footprint Height and Elevation (*22*) metric product which identifies surface waveforms with high fidelity.

2. Only shots with a beam sensitivity >0.98 for tropical Evergreen Broadleaf Tree prediction strata, and beam sensitivity >0.95 elsewhere, were included. Beam sensitivity was calculated using a 3-sigma signal threshold and thresholds were selected to provide a sufficiently high signal-to-noise ratio to penetrate the highest canopy cover expected in these regions (*23*).

3. Shots with high degradation of geolocation performance were excluded from the sample since these may fall outside the geographic extent of a 1 km cell.

4. Orbit granules affected by low cloud/fog, which were identified using an iterative local outlier detection algorithm.

All surface waveforms were used to generate footprint biomass AGBD estimates and standard errors within a 1 km cell and these footprint estimates are provided in the GEDI L4A Footprint Biomass Product (*24*). Shots that were not land surface or that were designated as urban were assigned a zero mean / zero covariance model. Additionally, leaf-off shots in deciduous forests where the L4A predictor variables included RH metrics below the top-of-canopy were excluded from the sample, as GEDI's L4A models are not applicable to these conditions. See the L4B Gridded Biomass product (*25*) and its associated algorithm theoretical basis (ATBD) document (GEDI_ATBD_L4B) for more details on the aforementioned data product flags and algorithms used for quality filtering and model assignment.

Not every 1 km cell has a biomass estimate currently due to incomplete spatial coverage as the result of persistent clouds in some areas and the orbital dynamics of the ISS. During the 1st year of GEDI's mission, the ISS was in a randomly precessing orbit and had relatively uniform spatial coverage as a function of longitude. The ISS was subsequently raised to an orbit approximately 16 km higher in early 2020 which resulted in a 4-day repeat cycle. This caused both a clustering of its observations along its orbital track and left unexpected gaps across track (Fig. S2). One requirement of hybrid estimation is that there be at least two tracks per cell for variance calculation. Consequently, biomass was not estimated for cells with only one track because the associated standard error could not be calculated. While GEDI's sampling to date leaves substantial areas without estimates at the 1 km scale, 6 km estimates may be made almost everywhere. For estimates presented here beyond the 1 km scale, we applied straightforward

aggregation, with attention to sampling and model dependencies to 6 km hybrid mean estimates and uncertainties.

The AGBD predictions for each waveform come from the GEDI L4A product which applies linear models to each *plant functional type x world region* combination within the latitudes covered by the ISS.  Parametric models are currently required for hybrid model-based inference (*26*).  Specifically, the variance estimators described combine sampling uncertainty— representing how well GEDI covers the area of interest—with modeling uncertainty, which is quantified by the parameter covariance matrix produced through the footprint-level modeling process.  GEDI's L4B Gridded Biomass product is the application of hybrid estimators to the shots within 1 km grid cells across Earth's tropical and temperate terrestrial ecosystems.

As with any formal mode of inference, it is important to list assumptions associated with hybrid inference.  First, the footprint-level AGBD model and its parameter covariance matrix are assumed to apply to the areas where they are used.  Training data should ideally represent the range of conditions found in the modeled population (*27*).  Practically, this assumption will be violated to some degree in parts of the world's ecosystems, resulting in a bias for which the estimator does not account.  Secondly, our hybrid variance estimator does not account for model residual error on the assumption that it is negligible when the area of interest is large enough.  The residual error of a large number of predictions from a well-fit model should sum to near zero; simulations suggest that a 1 km area is typically large enough to support the assumption of negligible residual variance. (*28*) A third assumption is that GEDI's sample conforms to the properties of a randomly allocated cluster sample.  Flight lines are conventionally treated as cluster samples with airborne lidar samples (*29*) and we assume that missing waveforms (most frequently due to clouds) are the result of a random process.

GEDI's estimators do not account for varying probabilities of inclusion in the sample measured by the instrument. Thus, if an estimate is required for an area large enough to exhibit different sampling probabilities, estimates must be aggregated from smaller areas where sampling probability is uniform. For example, differential cloud cover makes GEDI's sample of the rainforests of Brazil sparser than the sample of the savannas in the country's Cerrado region. ISS orbital crossings are also at their sparsest at the equator. The mission's orbital resonance problem created an additional source of irregularity in sampling probability. These factors (uneven cloud cover, ISS orbital track density) are assumed here to be invariant at the scale of 1 km cells. For estimates of larger areas such as countries, we require an intermediate, aggregable estimation scale for which sampling probability may be assumed to be approximately uniform. Since the swath width of GEDI's 8 beams is 4.8 km, we concluded that intermediate estimates for 6 km grid cells ("tiles") would adequately mitigate varying sample intensity caused both by orbital resonance and broader latitude- and cloud-based factors, while minimizing the number of tiles with fewer than two tracks. Supplemental Methods section Aggregating Tile-level Estimates to Larger Areas details our methods of aggregating estimates from 6 km tiles under the hybrid inference paradigm. These methods account for the possibility of using multiple L4A models within a single tile and elaborate methods to consider dependencies when multiple tiles are combined to create mean and variance estimates over large areas, such as countries or the U.S. FIA hex estimates presented here.

**USFS FIA estimates**

We obtained FIA estimates of AGBD, AGB and the proportion of forest using a fine-scale equal-area hexagonal tessellation covering the conterminous US. The FIA hexagon estimates were published as a comprehensive biomass dataset (*30*) for validation of remotely sensed biomass estimation at the finest spatial resolution available from the FIA database. Included in the dataset are the FIA's estimate of AGBD across the entire land area within each hexagon, along

with the standard error of the estimate, the proportion of forested area, and the number of FIA plots used to make the estimate. The standard errors were then used to create confidence intervals for each hexagon and to assess the difference of means between GEDI and FIA. We used the values of aboveground live biomass based on the Jenkins et al. (*31*) allometries to ensure a similar comparison to GEDI's AGBD estimates, which use these same allometries.

On average there were 28 FIA plots per hexagon, with the vast majority having between 20 and 30 plots. The total number of plots across all hexagons was 338,451. GEDI footprint-level observations varied by latitude, with more coverage away from the equator, and by longitude as a function of the ISS orbital ground track with an average of ~20,000 footprints per hexagon, though some hexagons could exceed 100,000 footprints.

GEDI mean AGBD value for a hexagon was compared with the FIA estimate using a test statistic (see McRoberts et al. (*32*), Eq. 3c) for a difference of means:

$$t = \frac{\hat{\mu}_{FIA} - \hat{\mu}_{GEDI}}{\sqrt{M\hat{S}E(\hat{\mu}_{FIA}) + M\hat{S}E(\hat{\mu}_{GEDI})}} \tag{1}$$

where $\hat{\mu}_{FIA}$ and $M\hat{S}E(\hat{\mu}_{FIA})$ are the estimated mean AGBD and mean square error from the FIA design-based plots within a hexagon, and $\hat{\mu}_{GEDI}$ and $M\hat{S}E(\hat{\mu}_{GEDI})$ are the corresponding values from hybrid estimation using the GEDI AGBD values within the same hexagon. While formal hypothesis tests based on a specific confidence level could be performed, the value of such tests has been questioned (*33*) and in our case may be overly constraining where the goal is to use observed departures from the validation data as a guide towards discovering potential biases. Hence, we chose to report only the value of the test statistic (shown in Fig. 9) rather than whether the test statistic exceeded some value based on a set confidence level.

**Country estimates**

National-scale GEDI estimates of land surface mean AGBD and the associated standard error were calculated within country boundaries delineated by a 10-meter resolution vector dataset (*34*). National-scale NFI estimates of AGBD were taken from the 2020 Global Forest Resources Assessment (*35*) (FRA) published by the Food and Agriculture Organization (FAO) of the United Nations.  This report is a global evaluation of forests, focusing on the state of forest resources and emerging trends from the past 30 years.  FAO estimates are only for forested lands, whereas GEDI estimates are for all lands. Therefore, to ensure a similar comparison to GEDI-based estimates we retrieved estimates of AGBD of forested land, the area of forested land, and total land area for every available country in the FRA online database.  We used these values to calculate each country's total land AGBD and total AGB, as follows: total AGB was determined by multiplying the forested AGBD by the area of forested land, and the country mean AGBD was calculated by dividing total AGB by the total country land area.  For example, a country with an area of 150,000 km2 that is 40% forested with a forested AGBD of 260 Mg/ha has a country-level mean AGBD of 104 Mg/ha, and a total AGB of 1.56 Pg.  Note that in deriving the total land AGBD and AGB using FAO data we assume there is no biomass on non-forest land, which is the same assumption made in the U.S. FIA estimates.

The country-level comparisons include all countries located entirely within the ISS orbital extent (51.6 °N & °S) that the FRA included in its 2020 report.  Large countries with a vast majority of land area within the ISS extent were also included, even if not entirely within the extent; specifically, China, Argentina, and Chile.  The United States was also included but is a special case because of Alaska. The US estimate in the FRA report includes data from Alaska, but because the GEDI instrument does not sample any part of Alaska, we used the most recent FIA estimates for the US and its territories in place of the values presented in the FRA report.  We did this by summing the hexagon-level total biomass (*30*) (AGB) to get a total biomass for the

coterminous U.S. as reported above, and for the non-conterminous U.S we used AGB values reported by the FIA. We then divided the total AGB by the total U.S. land area (excluding Alaska) to arrive at a total AGBD that is comparable to the GEDI estimate. We used FIA estimates to calculate the proportion forest value for the U.S. For country level estimates, only shots with a beam sensitivity >0.98 across all prediction strata were used to avoid systematic differences between prediction strata in the fraction of 6 km cells with fewer than two tracks.

# Results

## Pantropical and Temperate Biomass Estimates at 1 km Resolution

Mean aboveground biomass density estimates and their standard errors (SE) were created from the GEDI footprint level biomass estimates over a 1 km grid (Fig. 1). Biomass density had a mean of 108.9 Mg/ha for 1 km cells whose predominant plant functional type (PFT) class was forest. Values of AGBD varied considerably by PFT with evergreen broadleaf forests (EBT) showing the largest mean value (126.7 Mg/ha) and grassland/savanna/woodland (GSW) the lowest with a mean of 9.5 Mg/ha (Fig. 2 and Table S1). When considered by PFT and world region, EBT forests of North Asia had the largest AGBD with a value of 167.6 Mg/ha.
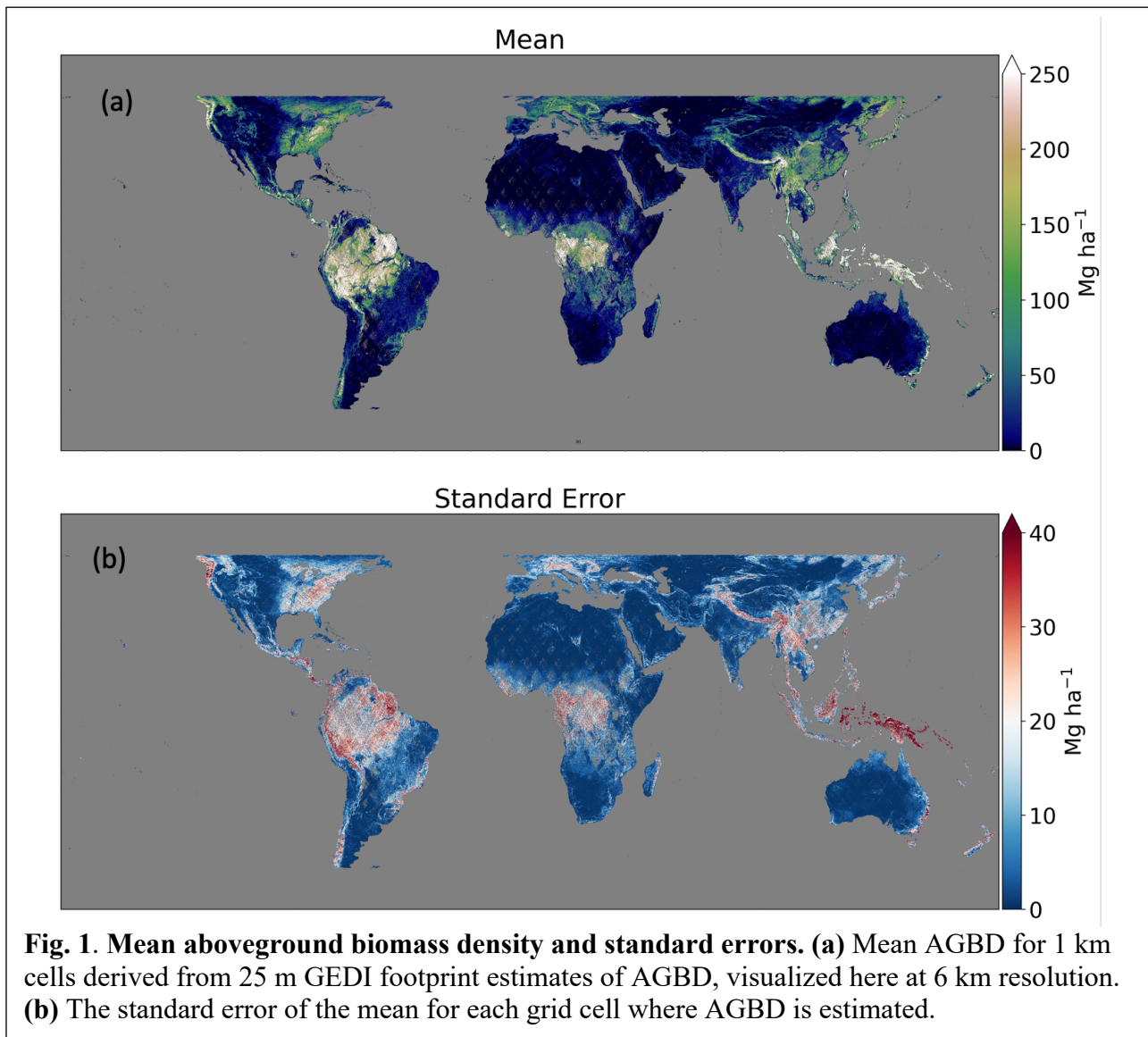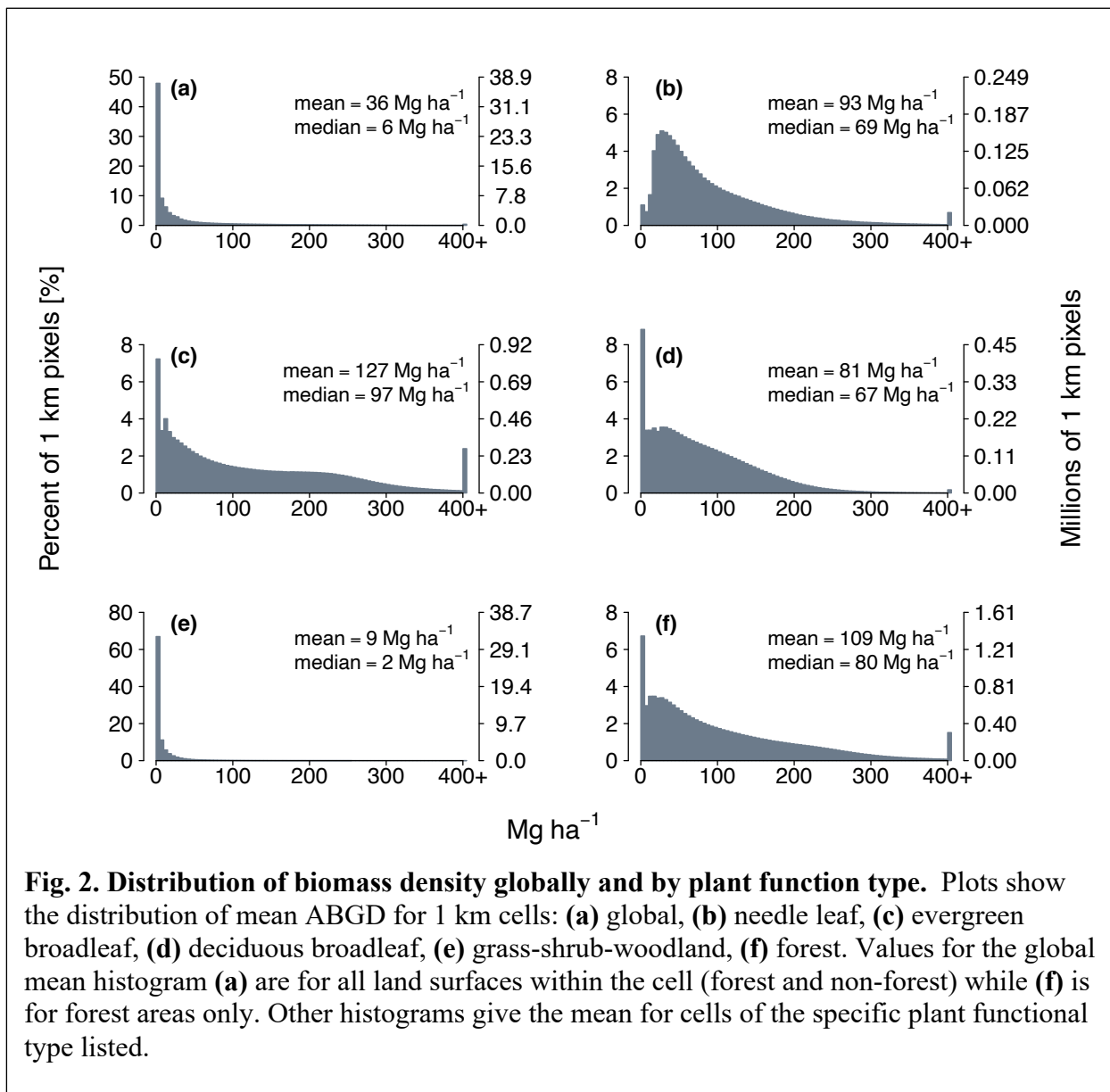


**Fig. 1**. **Mean aboveground biomass density and standard errors. (a)** Mean AGBD for 1 km cells derived from 25 m GEDI footprint estimates of AGBD, visualized here at 6 km resolution. **(b)** The standard error of the mean for each grid cell where AGBD is estimated.

GEDI was designed to meet stated precision requirements; specifically, that 80% of the 1 km land surface cells on the land surface between 51.6° N&S must have a standard error of the mean of <= 20% for cells where AGBD > 100 Mg/ha and < 20 Mg/ha for cells where AGBD <= 100 Mg/ha (*18*). As described above, there must be at least two tracks through a cell for variance estimation.  It is therefore useful to describe error statistics with respect to (a) the percentage of those cells that have met the observational requirements and (b) all cells in total (the latter on which the GEDI formal requirements are based).  For the land surface as a whole (between 51.6° N&S) GEDI had sufficient observations (two or more tracks) in 74.2% of the 1 km cells (Fig.



**Fig. 2. Distribution of biomass density globally and by plant function type.** Plots show the distribution of mean ABGD for 1 km cells: **(a)** global, **(b)** needle leaf, **(c)** evergreen broadleaf, **(d)** deciduous broadleaf, **(e)** grass-shrub-woodland, **(f)** forest. Values for the global mean histogram **(a)** are for all land surfaces within the cell (forest and non-forest) while **(f)** is for forest areas only. Other histograms give the mean for cells of the specific plant functional type listed.

S2) and 70.4% of all land surface cells meet the GEDI biomass requirements for standard error of the mean. Considering only those cells with sufficient observations, 77.3% of the high biomass cells meet requirements, and 97.2% of the low biomass cells meet requirements, and for both ranges collectively 94.8% met requirements (Fig. 3). Standard errors of mean AGBD for high biomass cells were generally below 20% with an average of 15.2% but with some relatively small variations by PFT (Fig. S3) and region (Fig. S4). The one exception was the GSW PFT
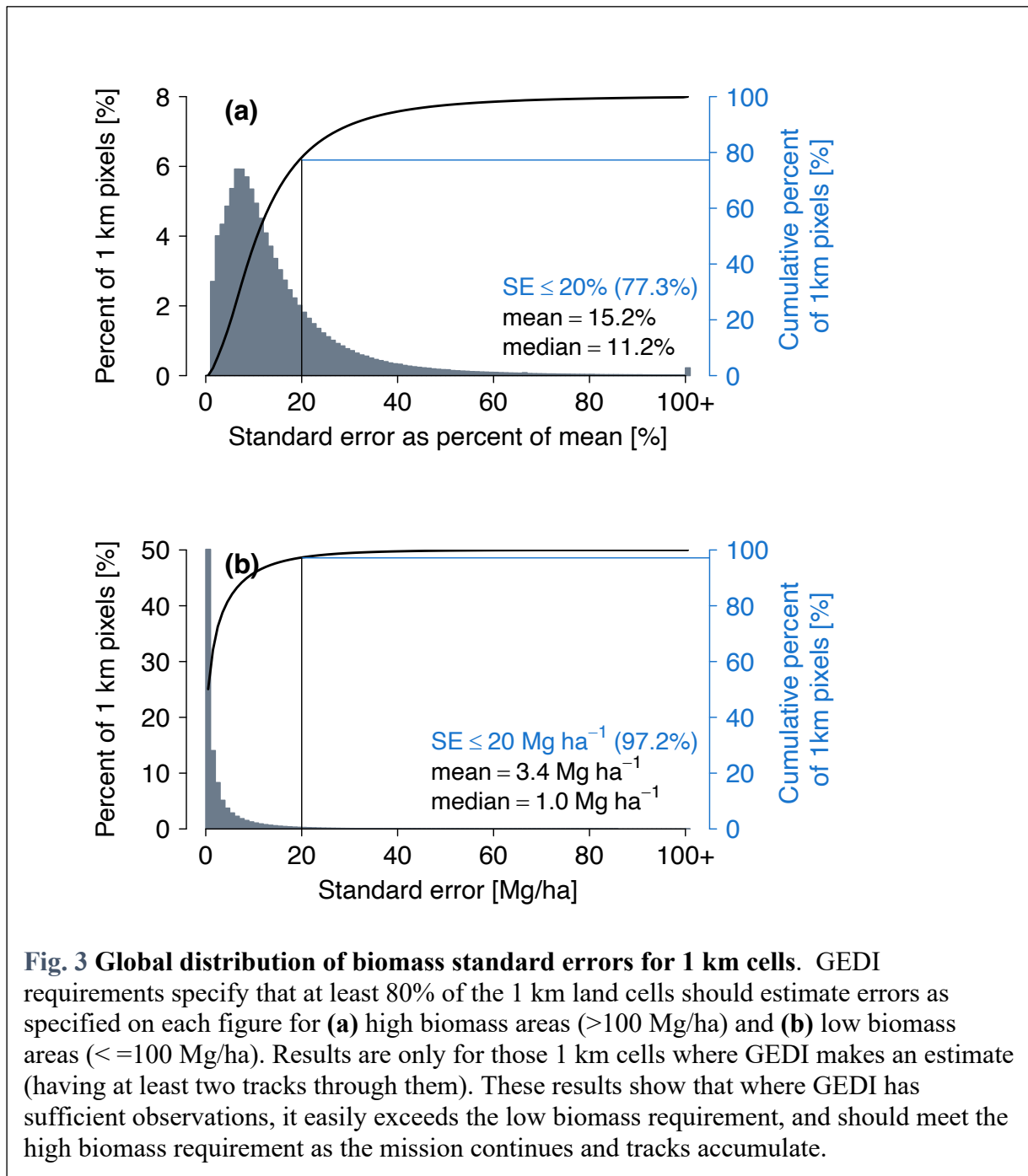


**Fig. 3 Global distribution of biomass standard errors for 1 km cells**. GEDI requirements specify that at least 80% of the 1 km land cells should estimate errors as specified on each figure for **(a)** high biomass areas (>100 Mg/ha) and **(b)** low biomass areas (< =100 Mg/ha). Results are only for those 1 km cells where GEDI makes an estimate (having at least two tracks through them). These results show that where GEDI has sufficient observations, it easily exceeds the low biomass requirement, and should meet the high biomass requirement as the mission continues and tracks accumulate.

which showed a mean error of 30.8% but noting that the values of AGBD are also much lower for this PFT.  For the lower biomass range, the average standard error was 3.4 Mg/ha.

## Country-Level Estimates

We next found AGB for countries whose borders were within the latitudinal limits of ISS observation (Fig. 4a), with minor exceptions for China, Chile, and Argentina where only a small part of the country is beyond 51.6° N or S and excluding Alaska for the United States. Total biomass stocks were then compared with those from the FAO (Fig. 4b). While GEDI estimates of AGB were strongly correlated with FAO estimates ($r^2$ = 0.86, RMSD = 3.2 Pg; Fig. 5), GEDI's biomass totals trended slightly higher with an average difference (FAO – GEDI) of -0.63 Pg. For two countries, China, and Indonesia, GEDI's total AGB were considerably larger at 27.7 Pg and 23.3 Pg respectively. Relative standard errors for AGBD at the country level had a mean of 7.7% and a median of 3.9%. GEDI and FAO estimates of AGB, AGBD and their standard errors for observed countries are given in Table S2.

GEDI does not observe the entire global land surface, so it is not possible to estimate total AGB for the Earth. Additionally, due to data availability issues, FAO does not provide an estimate for every country where there is a GEDI estimate. For those 169 countries with both a GEDI and FAO estimate, the GEDI estimated total biomass was 480.2 Pg. FAO estimates for these same countries totalled 373.1 Pg, a total difference of 107.1 Pg. Thus, GEDI estimates about 29% more AGB for the tropical and temperate land surface compared to FAO estimates. This difference is related, in part, to the fact that GEDI measures the biomass of both forest and non-forest areas, whereas FAO estimates are only for those areas denoted as forest (>10% canopy

**Fig. 4. GEDI country-wide estimates of AGB as compared with in-country reports**. **(a)** GEDI estimates. **(b)** FAO estimates. **(c)** Difference (FAO – GEDI). GEDI estimates AGB across all land, not just forested land, while FAO estimates are focused on forests. The national forest inventories used as the basis of FAO's estimates vary widely in terms of framework, quantity, and quality.
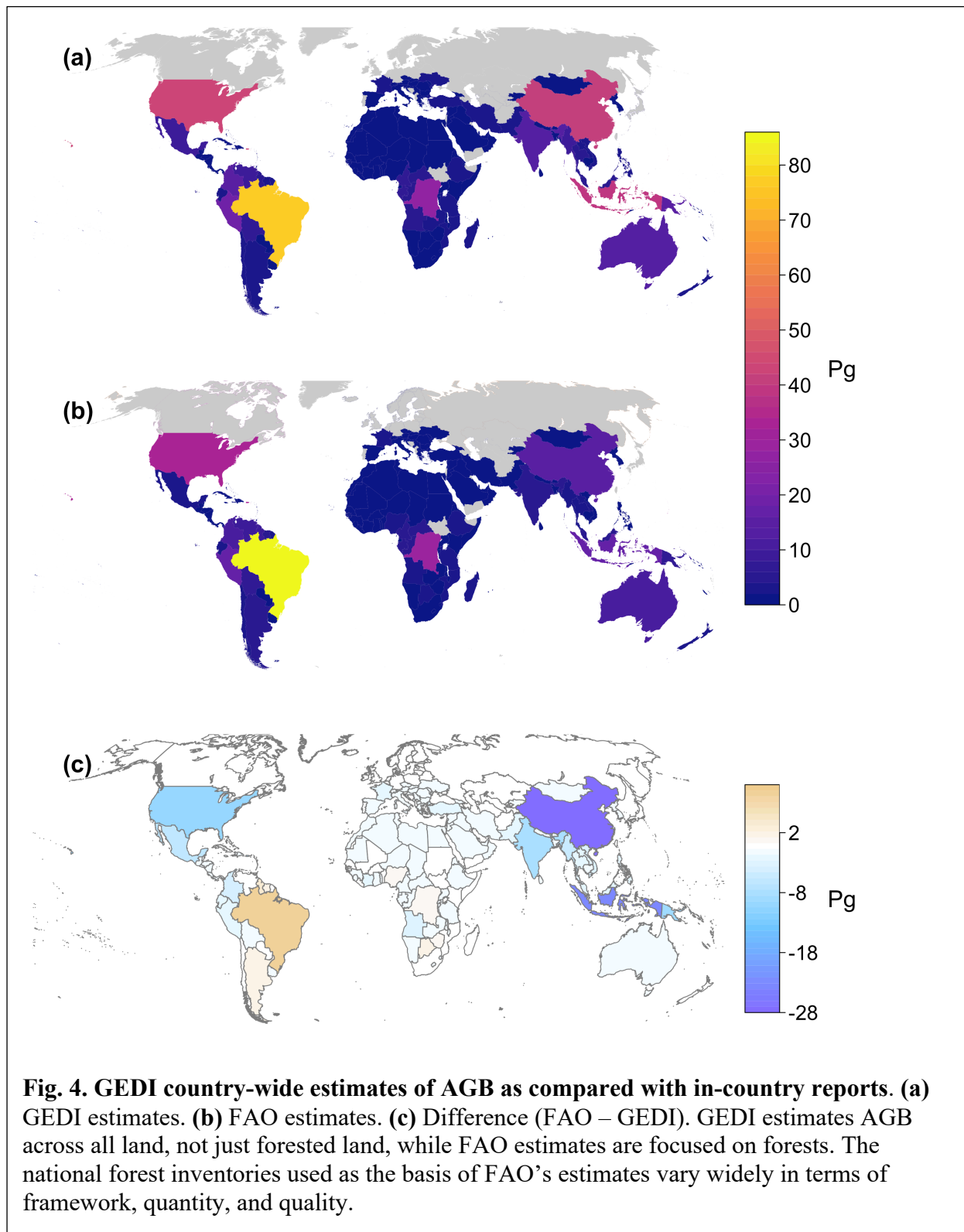
cover of minimum 5 m height over 0.5 ha area). Incomplete filtering of anomalous waveform

data, topographic artefacts, and model misspecification can also result in estimates of AGB that

are too large from GEDI. These issues are addressed in GEDI data processing and are further considered in the Discussion section.
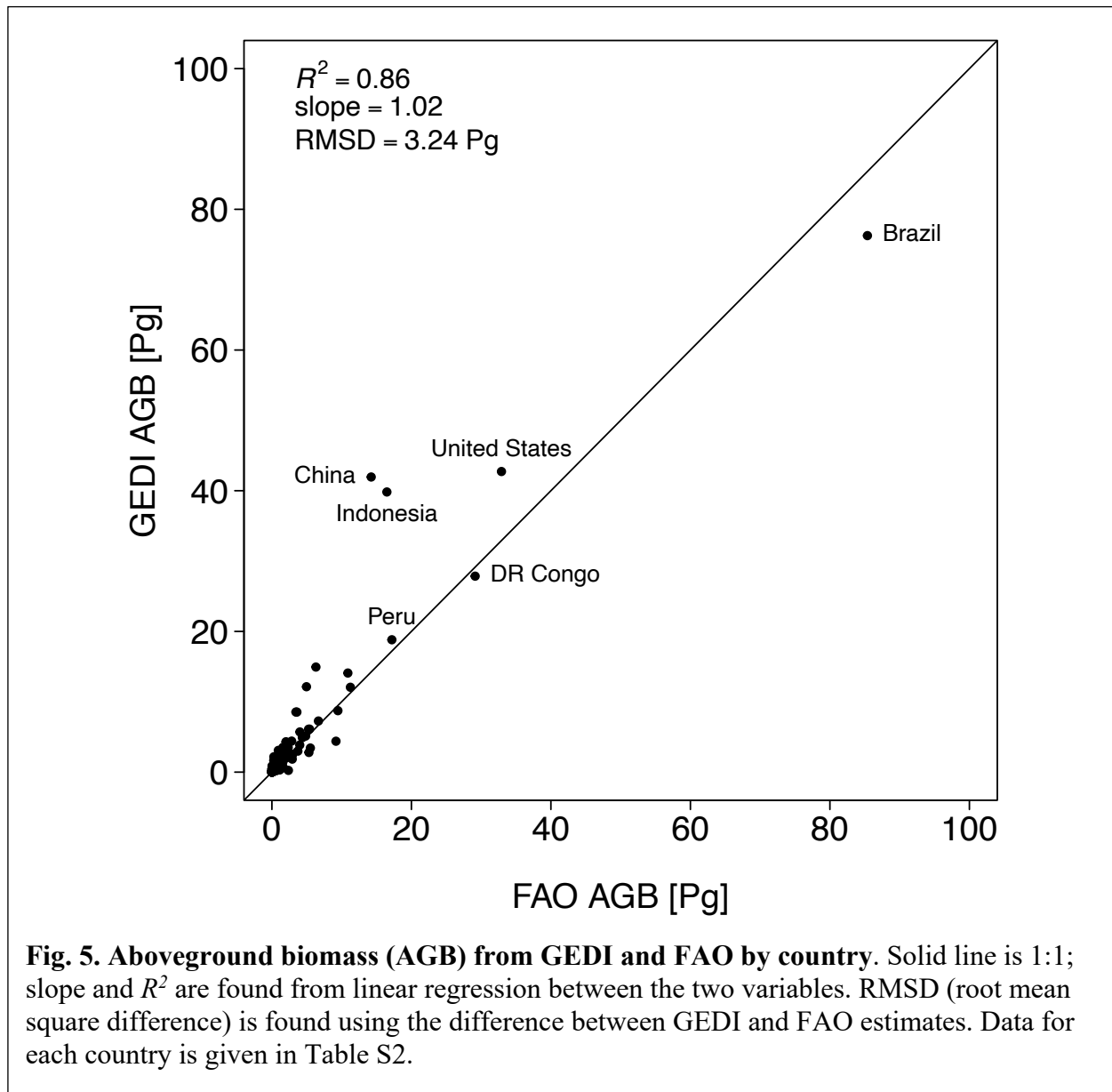


**Fig. 5. Aboveground biomass (AGB) from GEDI and FAO by country**. Solid line is 1:1; slope and $R^2$ are found from linear regression between the two variables. RMSD (root mean square difference) is found using the difference between GEDI and FAO estimates. Data for each country is given in Table S2.

Biomass density showed more variability than total biomass in comparisons with FAO ($R^2$ = 0.57, RMSD = 47.7 Mg/ha) but the relationship was influenced by a few outliers from smaller countries (Fig. S5). GEDI estimates were mostly higher than FAO, with 126 of the 169 countries assessed having higher AGBD from GEDI. This is again related to the factors listed above as well as the differences in how the densities are calculated. GEDI estimates are the average density over all lands, whereas FAO densities are the total biomass of lands supporting biomass,

as reported by FAO, divided by the total area of the country (not just forested lands), which necessarily must lead to lower estimates of AGBD from FAO. Standard errors of mean AGBD were small with a mean of 3.4 Mg/ha (Fig. 6). Errors exceeding 5 Mg/ha occurred almost exclusively over small island nations having incomplete sampling and low biomass stocks. Two notable exceptions were Indonesia and Papua New Guinea which had AGBD errors of 7.3 Mg/ha and 19.3 Mg/ha, respectively (Fig. 7).
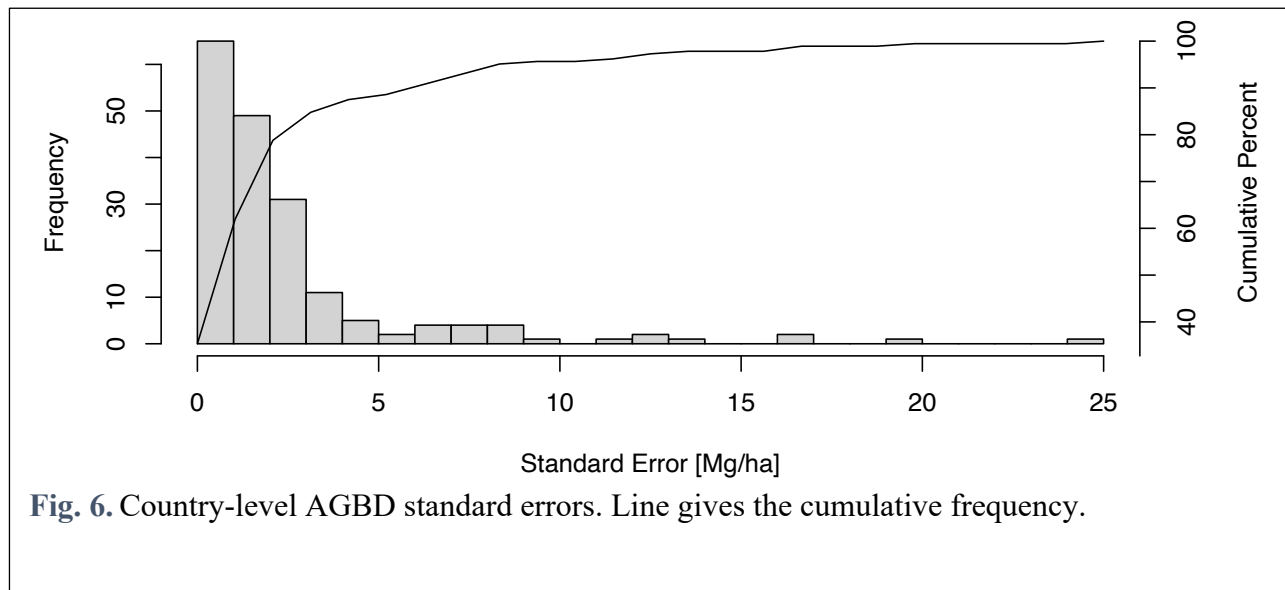


**Fig. 6.** Country-level AGBD standard errors. Line gives the cumulative frequency.
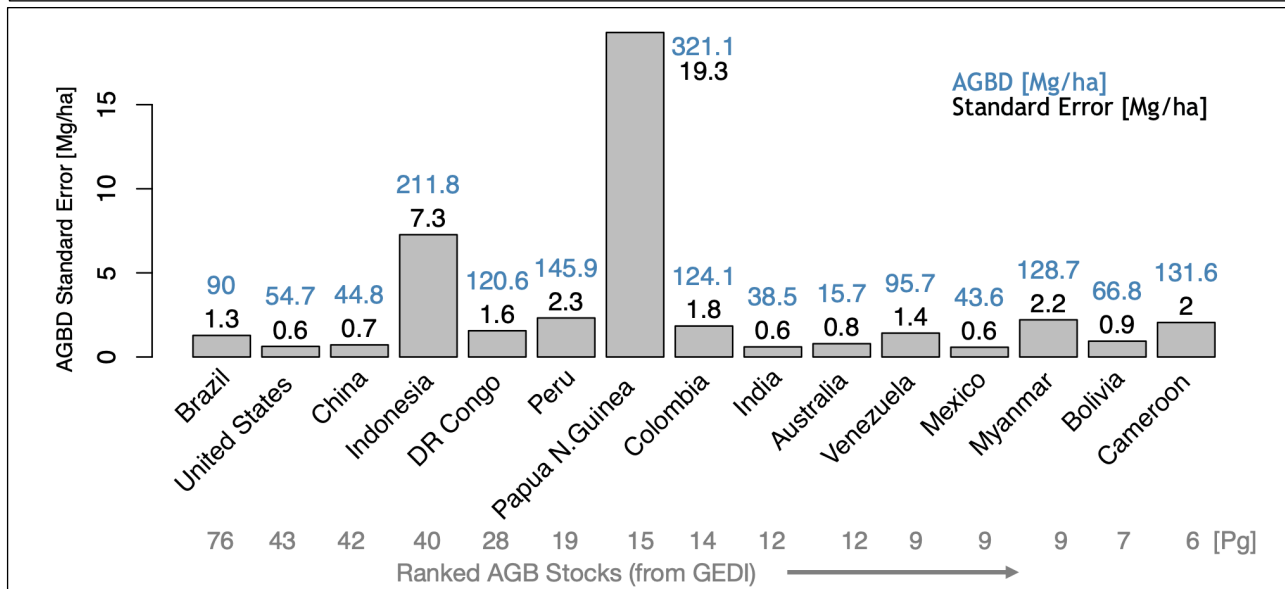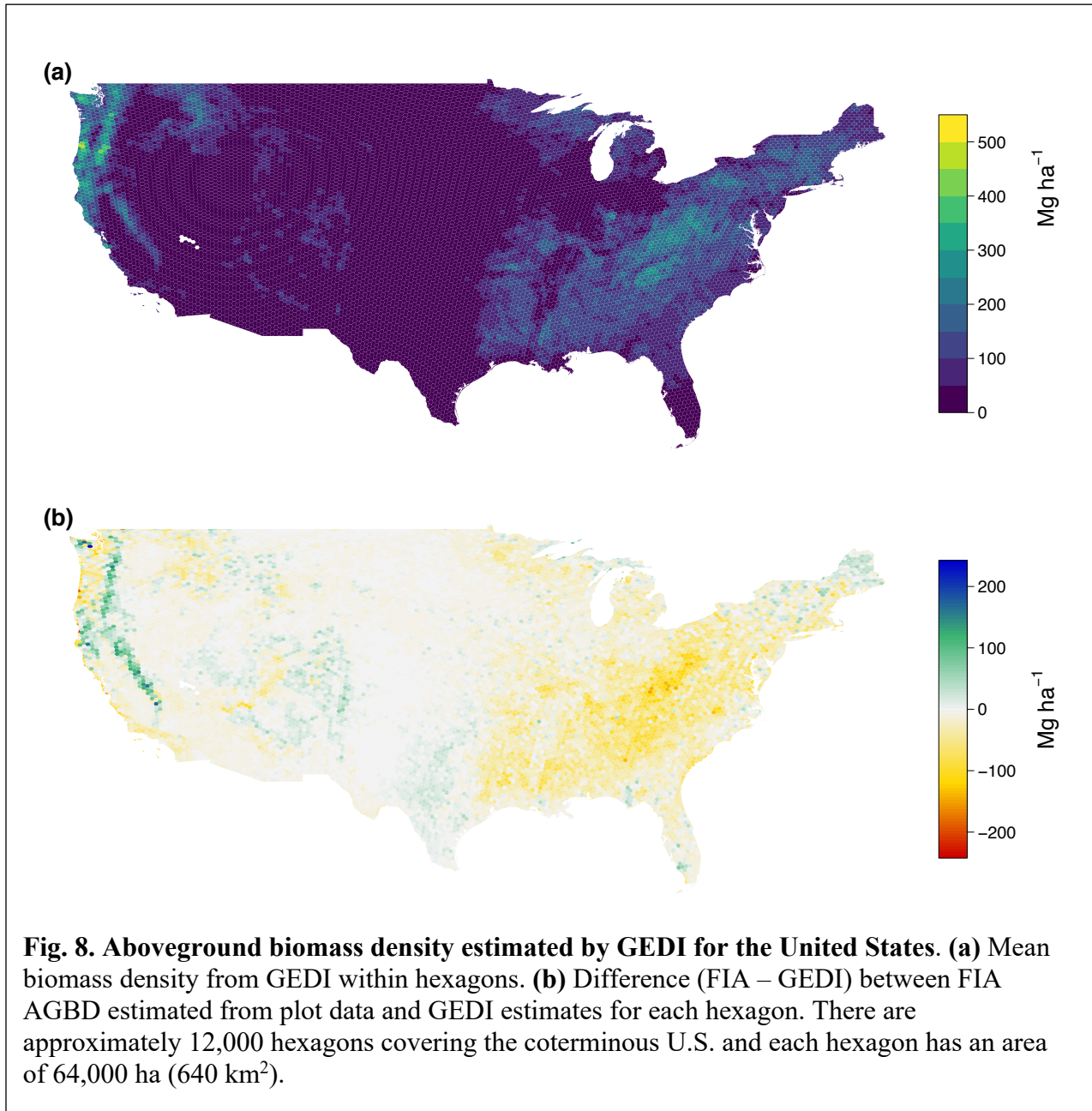


**Fig. 7.** Standard errors for countries with the 15 largest biomass stocks (AGB) as estimated from GEDI. Above each bar is given the GEDI AGBD (blue) and its standard error (black). Stocks for each country are given below the country name.

## Comparison with U.S. National Forest Inventory Data

We applied hybrid inference with GEDI data to 64,000-ha hexagons covering the United States and compared our estimates to those derived from the USFS FIA plots (Fig. 8). There are some systematic differences apparent between the two: GEDI estimates of AGBD were low relative to FIA data in the conifer dominated PFT of the Pacific Northwest and northern East Coast regions while the mixed broadleaf forests of the Eastern U.S mountainous areas showed consistently higher AGBD in comparison to FIA. For the U.S. hexagons, GEDI data compare well to FIA estimates, with $r^2$ = 0.81, RMSD = 28.3 Mg/ha, and the slope of the relationship equal to 0.99 (Fig. 9a). GEDI estimated an average AGBD of 52.6 Mg/ha and AGB of 3.2 Tg per hexagon. The equivalent FIA estimates were AGBD of 41.9 Mg/ha and AGB 2.6 Tg, bearing in mind that FIA only measures biomass on lands meeting its definition of forest but density here was calculated as a function of the entire land surface area of the hexagon. The mean AGB difference (FIA – GEDI) was -0.64 Tg; GEDI thus estimates about 24.3% more biomass stock in the U.S. relative to the FIA total. This histogram of differences is negatively skewed reflecting the larger GEDI values in Eastern U.S. (Fig. 9b) and a direct comparison of quantiles shows both that GEDI estimates tend larger than FIA for values of AGBD below around 250 Mg/ha and smaller for values above that. Note that in contrast to country comparisons, there is little difference in the patterns and relationships using AGB or AGBD relative to FIA because the land area of every hexagon is the same, aside from a few on the coasts or the borders with Canada and Mexico.

**Fig. 8. Aboveground biomass density estimated by GEDI for the United States**. **(a)** Mean biomass density from GEDI within hexagons. **(b)** Difference (FIA – GEDI) between FIA AGBD estimated from plot data and GEDI estimates for each hexagon. There are approximately 12,000 hexagons covering the coterminous U.S. and each hexagon has an area of 64,000 ha (640 km$^2$).

The standard errors of the mean from GEDI for hexagons as derived from hybrid estimation, along with the standard errors derived from the designed-based FIA network may be used to assess the likelihood that observed hexagon-level differences are meaningful (Fig. 9c) and to compare the precision of their mean estimates through their individual confidence intervals (Fig. 10).
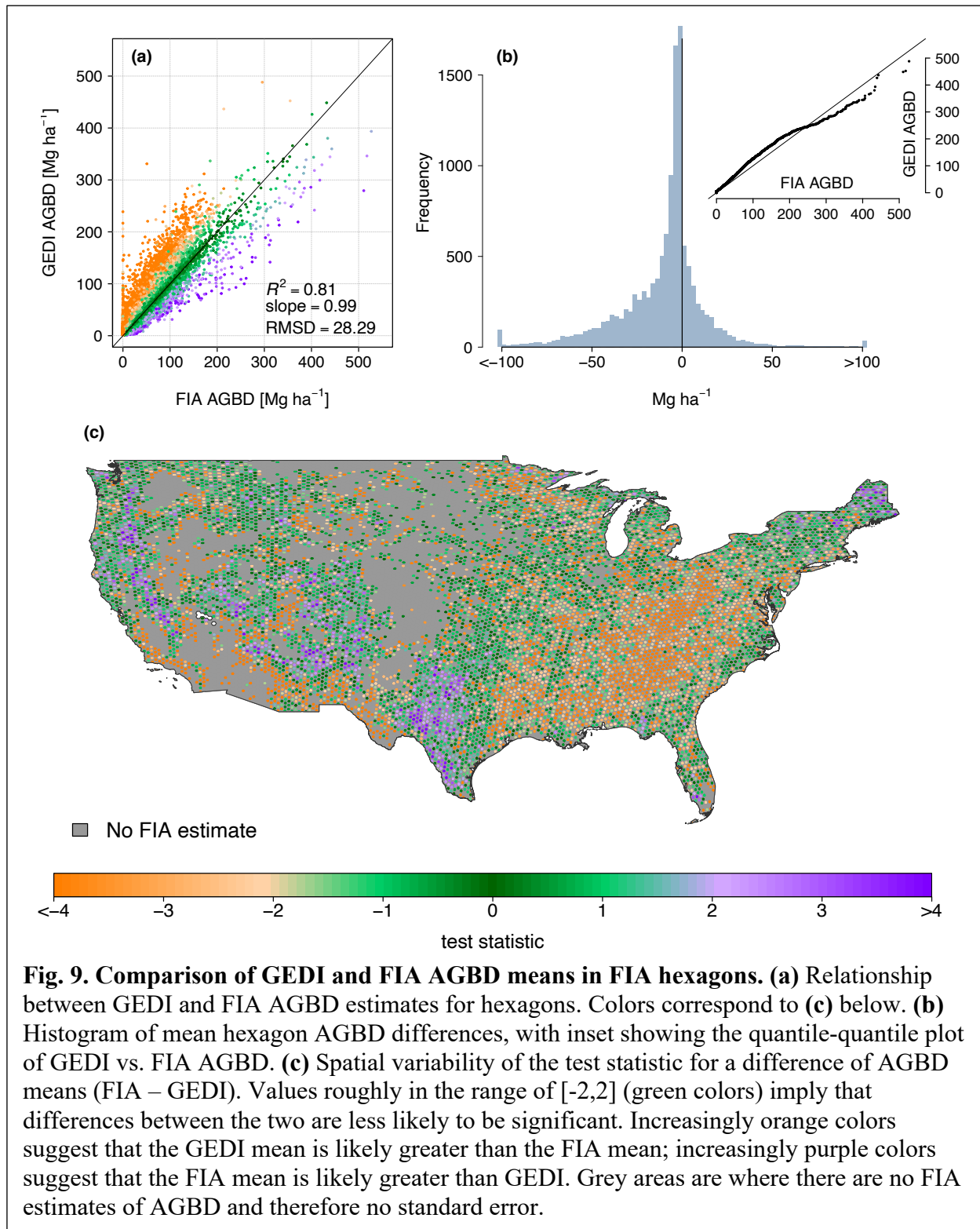
**Fig. 9. Comparison of GEDI and FIA AGBD means in FIA hexagons. (a)** Relationship between GEDI and FIA AGBD estimates for hexagons. Colors correspond to **(c)** below. **(b)** Histogram of mean hexagon AGBD differences, with inset showing the quantile-quantile plot of GEDI vs. FIA AGBD. **(c)** Spatial variability of the test statistic for a difference of AGBD means (FIA – GEDI). Values roughly in the range of [-2,2] (green colors) imply that differences between the two are less likely to be significant. Increasingly orange colors suggest that the GEDI mean is likely greater than the FIA mean; increasingly purple colors suggest that the FIA mean is likely greater than GEDI. Grey areas are where there are no FIA estimates of AGBD and therefore no standard error.

Approximately 21% of the hexagons did not have a confidence interval from FIA because the FIA AGBD estimate was zero. While the FIA assumes zero biomass for non-forest lands, GEDI estimates biomass for cells across all lands, and so has a non-zero biomass estimate for these.

The spatial distribution of a test statistic for the difference of means showed regional, systematic differences in estimated AGBD, most notably the Pacific Northwest and the Appalachian region of the Eastern U.S. GEDI generally has smaller confidence intervals about its means relative to FIA because it has many more observations within a hexagon as compared to FIA data. GEDI uncertainties also include a modelling error term from the calibration equations which is not present in FIA estimates. These modelling errors are not large and despite some dependence on the number of samples per tile and the number of models applied, remain relatively constant across scales, from 1 km cells to the areas of hexagons to entire countries. Note, however, that GEDI estimates of uncertainty do not account for any violations of the assumptions of hybrid inference, which may lead to biases and mean precisions and confidence ranges that are overly optimistic, discussed next.



**Fig. 10. The 95% confidence interval ranges for GEDI and FIA means at the hexagon scale.** While GEDI variance estimators include both a modeling component and a sampling component, GEDI has smaller intervals because it has many more footprint-level biomass predictions, thereby reducing sampling error relative to FIA which has about 28 field plots per hexagon. Note that Frequency (y-axis) is on a logarithmic scale. The few GEDI plots with ranges exceeding 50 Mg ha$^{-1}$ are partial hexagons located on the coastlines and international borders.

# Discussion

GEDI was conceived to provide the data on ecosystem structure required to address important questions about the Earth's forests, including quantifying the net impact of deforestation and subsequent regrowth on atmospheric $CO_2$ concentrations, among others. Key to these efforts is the creation of accurate maps of baseline carbon stocks of sufficient spatial resolution and with well-understand uncertainties that may be used to monitor changes through time and provide accurate initialization for prognostic studies of the impacts of land use and climate change.

Several aspects unique to GEDI set the mission and its resulting biomass maps apart from others that have been produced before. First, GEDI's biomass maps are based on GEDI data alone, and are not the product of fusion or spatial extrapolation with data from other sensors. Secondly, the models that relate waveform measurements, such as height to biomass, were created using the most extensive set of field and aircraft data yet compiled. Third, GEDI has provided vastly more observations of ecosystem structure than previously available; our study used over 5 billion of these estimates to make its products. Past studies using GLAS at country to global scales were based on one to two orders of magnitude less data (*12–14*). However, GEDI most fundamentally represents a turning point because of its focus on formalized inference. Specifically, while biomass products from previous satellites have assessed residual error uncertainty at the pixel level, GEDI recognizes the need to assess uncertainty when individual observations (pixels, for example) are combined to estimate biomass over a larger area. Residual error in that context has little relative impact compared to the uncertainty that arises due to estimating the parameters of the models linking field observations with GEDI metrics.

The model parameters themselves are a more relevant source of uncertainty under the model-based paradigm, as they affect all predictions in a systematic way. GEDI's hybrid model-based estimator explicitly accounts for uncertainty in the model-fitting process through the use of the

model's parameter covariance matrix (*21*). There are alternative methods for explicitly addressing the effects of model covariance upon population estimates for large areas; for example approaches involving bootstrapping have been proposed (*20).* The key is that GEDI is the first forest observation mission to embrace inference over large areas, employing an integrated design process to account for the instrument's sampling pattern, the fitting of biomass models, and the reporting of grid cell mean biomass estimates and their uncertainties. Previous remote sensing efforts that have ignored covariance among observations over large areas have had to rely upon ad hoc, and sometimes ambiguous, methods of uncertainty assessment (*26, 36*).

The precision requirement of the GEDI mission that 80% of 1 km cells not exceed a standard error of 20 Mg/ha or 20% of the mean AGBD (for low and high biomass levels, respectively) has not yet been met, due to changes in the ISS altitude, but as noted above, of those cells with the requisite two overpasses 95% meet the GEDI requirements. Substantial progress with respect to meeting the 80% mission goal is expected within the next year because: 1) the precision of GEDI's estimators is expected to increase rapidly as cells accumulate more than two overpasses (*21*); and, 2) recent changes to the ISS altitude are expected to substantially improve coverage of 1 km cells with no existing observations.

GEDI's variance estimates, accompanying the estimate of the mean for every 1 km cell, are crucial to monitoring progress toward the mission's precision goal. This cannot be achieved solely by validation using independent data. Validation using field data is not feasible globally and there are almost no 1 km field plots in any ecosystem, forested or otherwise. Comparison against 1 km estimates derived from airborne lidar is possible, however this process involves airborne estimates subject to some of the same model-related uncertainties affecting GEDI and would cover only a small fraction of the nearly 105 million grid cells over land in the study area. Direct comparisons with existing biomass maps are also difficult because they often have

differing resolutions and, as noted above, unclear statistical procedures to estimate uncertainty from pixels to some larger area - for example, comparing a 30 m biomass product to GEDI via aggregation of the 30 m pixels to 1 km – although progress continues to be made in this area (*32*).

Nevertheless, comparison against independent estimates of mean AGBD provide an opportunity to highlight potential problems with GEDI's current estimation process. Some degree of spread is to be expected in the hexagon- and country-level comparisons; field estimates have their own uncertainties, and important differences in definitions and allometric models can introduce large discrepancies among estimates that would otherwise be in agreement (*30*). Systematic differences between GEDI and reported estimates, though, suggest several issues worth exploring during GEDI's continued operations.

First, comparison with FAO data showed GEDI estimated more AGB for most countries. The UN FAO defines trees outside of forests and other wooded lands as those growing on lands with a combined cover of shrubs and trees of less than 10%, or tree cover less than 5%, or any trees growing in patches smaller than 0.5 ha or in urban or agricultural land. Such trees and patches are widespread in some areas (*37–39*) and represent biomass that is measured by GEDI but not by forest inventories. Application of standardized definitions of forest resulting in explicit and agreed upon forest/non-forest maps would enable refined comparisons. GEDI's footprint estimates of biomass could then be averaged only for forested areas for comparison to FAO estimates within countries.

Secondly, the footprint biomass calibration models linking field biomass to the GEDI waveforms are assumed under model-based estimation to be both properly specified and fitted with data representative of the areas to which the models will be applied (*27*). Estimated standard errors

may reflect a lack of fit with respect to available training data (for example somewhat lower $R^2$) but will not reflect biases in the selection of that data, and therefore potential biases in the calibration equations as applied. Comparisons with validation data can help reveal possible violations of the assumptions underlying model-based inference that are not revealed in the calibration model building process. For example, GEDI currently estimates far more AGB (a combined 51 Pg) in China and Indonesia than the countries themselves report (*35*). While these positive differences may be associated with the issue of non-forest biomass discussed above, we note that GEDI's AGBD calibration dataset is particularly sparse in Asia and therefore represents a potential source of bias. This lack of data in Asia may also help explain the relatively high standard errors for mean AGBD in Indonesia and Papua New Guinea; however, note that there is also a tendency for errors to increase as the magnitude of AGBD increases.

Similarly, comparison with FIA data in the western U.S. at the hexagon level reveals discrepancies that are, according to the respective confidence intervals, unlikely to be a result of sampling error on the part of GEDI or the field inventory. Some of these conifer systems may have biomass densities that exceed 2000 Mg/ha at the scale of GEDI footprints, and the calibration data set and derived calibration models (*40*) may not adequately represent the range of biomass present in this PFT as it occurs in these western montane regions. These examples indicate the need for additional data collection and a re-examination of the footprint biomass calibration models fitted for the region to refine GEDI's estimates of biomass for these areas. While improved model training in data sparse areas will help us better meet our assumptions, this may come at the cost of an increase in standard errors as potentially overly optimistic estimates are corrected.

Third, there is an assumption that the height metrics, as derived from the return waveform by GEDI algorithms, are unbiased and have errors that match pre-launch calibration analyses, e.g.,

1-2 m for canopy top height accuracy. The process of outlier detection, that is filtering of GEDI measurements to remove invalid data, while improving, is imperfect and errors in estimated biomass may remain. One example is misidentification of low-lying clouds that produce lidar waveforms that appear as tall canopy, an effect we noted in comparisons with FIA data in the ridge and valley complex of the Appalachians in the eastern United States. Steep topography also may lead to incorrect data interpretation. Over mostly bare-earth terrain with high slopes (generally exceeding about 15° to 20°), waveforms have vertical extents that may appear similar to canopies in GEDI algorithms yet provide spurious relative height metrics that are unrelated to real canopy height. This can lead to biomass estimates that are too large, say for very sparse woodlands, or estimates for areas that cannot support vegetation, such as deserts. For forested terrain, steep slopes may increase or decrease perceived canopy height based on canopy cover and tree distributions in the footprint (*41*). As GEDI outlier detection methods and waveform processing improve, such artifacts will decrease. For example, we have applied machine learning methods as an alternative to conventional waveform processing. Such methods have the potential to both increase accuracy but also provide improved error and outlier detection (*42*).

Comparisons such as these presented above are useful for highlighting potential modifications to biomass estimates as the mission progresses, and they also demonstrate the value of reliance upon an inferential framework where assumptions are clear and there are straightforward mechanisms through which violation of those assumptions may bias the estimates. In other words, because the framework allows for a direct estimate of the precision of its estimates, these may be used to flag deviations from validation data that are probabilistically unlikely and thus provide the means for detecting biases. As the mission works through these potential issues it may be that some new estimates of biomass are produced that are outside existing confidence intervals, reflecting a correction of bias in the process, as mentioned above. This is not a cause for concern; rather, it reflects the power of the GEDI approach.

Note that although many of the reported standard errors at the country level are small, for example 1.1% for the United States, these are in line with those reported by other studies (*14, 15*) that used methods related to our own. However, our approach, as with these other studies and almost all national forest inventories, does not consider model uncertainty from the allometric tree-level biomass models. Such uncertainty may be substantial, especially in tropical areas (*43*) where the data underpinning the models tend to be limited. Thus, a formally reported standard error, whether from a plot-based national inventory or one based on remote sensing, may be too optimistic considering these potentially larger allometric errors. Work is ongoing towards improving these allometric models, most recently using terrestrial lidar scanning (*44*).

## Future Directions and Conclusions

It may seem that building a remote sensing mission upon a formal mode of inference is limiting; that is, that the necessary design considerations may limit the flexibility of future applications using its data. However, the experience of GEDI thus far has illustrated just the opposite. The orbital resonance resulting from the ISS altitude in 2020 and beyond challenged the application of hybrid inference across large areas, e.g., areas of differential probability of inclusion within the sample are not addressed by the estimators described by Patterson et al. (*21*). The orbital problem accentuated variable sample intensity that developed due to both the differential presence of clouds and the latitudinal differences in overpass density. This disruption was accommodated relatively simply by applying the estimators at the broadest scales for which probabilities of selection could be presumed equal (6 km tiles) and using a weighted aggregation process while accounting for dependencies due to non-independent sampling and modeling errors. This is similar to weighted averaging of smaller-domain estimates practiced by field inventories when sample intensities vary over larger domains (*45*).

The parametric models and sample design used by GEDI also support a type of contingency approach applicable when a 1 km cell has not been intersected by at least two ground tracks, meaning that hybrid inference (which treats ground tracks as cluster samples) is not an option. Even by the end of the mission we expect some cells to still have incomplete coverage. Our contingency approach, Generalized Hierarchical Model-Based inference (GHMB) (*46*, *47*), uses two levels of models: one linking ground data and footprint scale lidar metrics (i.e. the footprint biomass calibration models) and one linking those footprint biomass predictions to wall-to-wall ancillary data. The GHMB framework uses probability theory under the model-based paradigm to appropriately combine uncertainty from the two models, as wall-to-wall predictions form the basis of a large-area estimate of biomass (*47–49*). Thus, the theory upon which GEDI's estimation of uncertainty is built can be extended to sensor fusion. For example, GHMB has been used with GEDI and wall-to-wall imagery from TanDEM-X (*50*), which provides interferometric synthetic aperture radar (SAR) from two orbiting satellites, to produce both height and biomass estimates for areas where no GEDI data exist, and at finer spatial resolutions than 1 km (*47*). One strong feature of GHMB is that models relating GEDI data to the wall-to-wall data may be locally calibrated. The GEDI team intends to use GHMB to provide gap-free biomass maps in subsequent data product releases. This framework further provides a pathway for fusion with the next generation of SAR missions with science goals related to biomass and disturbance dynamics, including the NASA ISRO Synthetic Aperture Radar mission (NISAR) (*51*) to be launched in 2024 and the ESA BIOMASS mission (*52*), scheduled for launch in 2023.

In conclusion, GEDI has demonstrated the value of an instrument dedicated to and optimized for the retrieval of ecosystem structure in general, and for biomass estimation in particular. The sheer volume of GEDI estimates of biomass is unprecedented, vastly outstripping the existing spaceborne lidar archive. GEDI's estimates continue to evolve as the instrument collects more data beyond its prime mission, and as footprint-level biomass models and their underlying

assumptions are refined in light of ongoing validation activities.  The results reported here represent a watershed product of the first space mission longitudinally coordinated, from engineering to estimation, to generate biomass products in a transparent way with errors that are well-characterized using established probability theory.  The GEDI investigation highlights the intrinsic value of an approach that explicitly address uncertainty as integral part of mission design.  As GEDI and future missions invest in formal modes of inference, they bring statistical rigor long employed by field surveys to a new generation of powerful, globally consistent monitoring tools.

# Acknowledgments

**Data and materials availability:** The GEDI footprint biomass data used to create the GEDI 1 km data product are available at the Land Processes Distributed Archive and Analysis Center (LPDAAC) as follows: GEDI L4A Footprint Level Aboveground Biomass Density, Version 2. (2021) doi: 10.3334/ORNLDAAC/1986.  The GEDI L4B 1 km gridded data set is available at the Land Processes DAAC: https://doi.org/10.3334/ORNLDAAC/2017. The GEDI country-level data are included in the Supplements. The GEDI results for mean and standard error of U.S. hexagons can be obtained by request from Ralph Dubayah.

# References

1.  Y. P. Seng, Historical Survey of the Development of Sampling Theories and Practice. *Journal of the Royal Statistical Society. Series A (General)*. **114**, 214 (1951).

2.  R. E. McRoberts, Satellite image-based maps: Scientific inference or pretty pictures? *Remote Sensing of Environment*. **115**, 715–724 (2011).

3.  G. Ståhl, S. Saarela, S. Schnell, S. Holm, J. Breidenbach, S. P. Healey, P. L. Patterson, S. Magnussen, E. Næsset, R. E. McRoberts, T. G. Gregoire, Use of models in large-area forest surveys: comparing model-assisted, model-based and hybrid estimation. *Forest Ecosystems*. **3** (2016), doi:10.1186/s40663-016-0064-9.

4.  G. Jia, E. Shevliakova, P. Artaxo, N. De Noblet-Ducoudré, R. Houghton, J. House, K. Kitajima, C. Lennard, A. Popp, A. Sirin, R. Sukumar, L. Verchot, in : *Climate Change and Land: an IPCC special report on climate change, desertification, land degradation, sustainable land management, food security, and greenhouse gas fluxes in terrestrial ecosystems*, P. R. Shukla, J. Skea, E. Calvo Buendi, V. Masson-Delmotte, H.-O. Pörtner, P. Roberts, D. C.Zhai, R. Slade, S. Connors, R. VanDiemen, E. Ferrat, M.Haughey, S. Luz, S.; Neogi, J. Pathak, M.; Petzold, J. Portugal Pereira, J. Vyas, P.; Huntley, Eds. (Potsdam, 2019), pp. 131–247.

5.  R. A. Houghton, F. Hall, S. J. Goetz, Importance of biomass in the global carbon cycle. *Journal of Geophysical Research: Biogeosciences*. **114** (2009), doi:10.1029/2009JG000935.

6.  M. C. Hansen, P. V Potapov, R. Moore, M. Hancher, S. A. Turubanova, A. Tyukavina, D. Thau, S. V Stehman, S. J. Goetz, T. R. Loveland, A. Kommareddy, A. Egorov, L. Chini, C. O. Justice, J. R. G. Townshend, *Science*, in press, doi:10.1126/science.1244693.

7.  A. Tyukavina, A. Baccini, M. C. Hansen, P. V. Potapov, S. V. Stehman, R. A. Houghton, A. M. Krylov, S. Turubanova, S. J. Goetz, Aboveground carbon loss in natural and managed tropical forests from 2000 to 2012. *Environ. Res. Lett.* **10**, 074002 (2015).

8.  G. C. Hurtt, R. Dubayah, J. Drake, P. R. Moorcroft, S. W. Pacala, J. B. Blair, M. G. Fearon, BEYOND POTENTIAL VEGETATION: COMBINING LIDAR DATA AND A HEIGHT-STRUCTURED MODEL FOR CARBON STUDIES. *Ecological Applications*. **14**, 873–883 (2004).

9.  G. P. Asner, J. Mascaro, H. C. Muller-Landau, G. Vieilledent, R. Vaudry, M. Rasamoelina, J. S. Hall, M. van Breugel, A universal airborne LiDAR approach for tropical forest carbon mapping. *Oecologia*. **168**, 1147–1160 (2012).

10. M. A. Wulder, J. C. White, R. F. Nelson, E. Næsset, H. O. Ørka, N. C. Coops, T. Hilker, C. W. Bater, T. Gobakken, Lidar sampling for large-area forest characterization: A review. *Remote Sensing of Environment*. **121**, 196–209 (2012).

11. V. Avitabile, M. Herold, G. B. M. Heuvelink, S. L. Lewis, O. L. Phillips, G. P. Asner, J. Armston, P. S. Ashton, L. Banin, N. Bayol, N. J. Berry, P. Boeckx, B. H. J. de Jong, B. Devries, C. A. J. Girardin, E. Kearsley, J. A. Lindsell, G. Lopez-Gonzalez, R. Lucas, Y. Malhi, A. Morel, E. T. A. Mitchard, L. Nagy, L. Qie, M. J. Quinones, C. M. Ryan, S. J. W. Ferry, T. Sunderland, G. V. Laurin, R. C. Gatti, R. Valentini, H. Verbeeck, A. Wijaya, S. Willcock, An integrated pan-tropical biomass map using multiple reference datasets. *Global Change Biology*. **22**, 1406–1420 (2016).

12. S. S. Saatchi, N. L. Harris, S. Brown, M. Lefsky, E. T. A. Mitchard, W. Salas, B. R. Zutta, W. Buermann, S. L. Lewis, S. Hagen, S. Petrova, L. White, M. Silman, A. Morel, *Proceedings of the National Academy of Sciences*, in press, doi:10.1073/pnas.1019576108.

13. A. Baccini, S. J. Goetz, W. S. Walker, N. T. Laporte, M. Sun, D. Sulla-Menashe, J. Hackler, P. S. A. Beck, R. Dubayah, M. A. Friedl, S. Samanta, R. A. Houghton, Estimated carbon dioxide emissions from tropical deforestation improved by carbon-density maps. *Nature Climate Change*. **358**, 230–234 (2012).

14. R. Nelson, H. Margolis, P. Montesano, G. Sun, B. Cook, L. Corp, H. E. Andersen, B. DeJong, F. P. Pellat, T. Fickel, J. Kauffman, S. Prisley, Lidar-based estimates of aboveground biomass in the continental US and

Mexico using ground, airborne, and satellite observations. *Remote Sensing of Environment*. **188**, 127–140 (2017).

15. H. A. Margolis, R. F. Nelson, P. M. Montesano, A. Beaudoin, G. Sun, H.-E. Andersen, M. A. Wulder, Combining satellite lidar, airborne lidar, and ground plots to estimate the amount and distribution of aboveground biomass in the boreal forest of North America. *Canadian Journal of Forest Research*. **45**, 838–855 (2015).

16. S. P. Healey, P. L. Patterson, S. Saatchi, M. A. Lefsky, A. J. Lister, E. A. Freeman, A sample design for globally consistent biomass estimation using lidar data from the Geoscience Laser Altimeter System (GLAS). *Carbon Balance and Management*. **7**, 1–9 (2012).

17. E. T. A. Mitchard, T. R. Feldpausch, R. J. W. Brienen, G. Lopez-Gonzalez, A. Monteagudo, T. R. Baker, S. L. Lewis, J. Lloyd, C. A. Quesada, M. Gloor, H. ter Steege, P. Meir, E. Alvarez, A. Araujo-Murakami, L. E. O. C. Aragão, L. Arroyo, G. Aymard, O. Banki, D. Bonal, S. Brown, F. I. Brown, C. E. Cerón, V. Chama Moscoso, J. Chave, J. A. Comiskey, F. Cornejo, M. Corrales Medina, L. Da Costa, F. R. C. Costa, A. Di Fiore, T. F. Domingues, T. L. Erwin, T. Frederickson, N. Higuchi, E. N. Honorio Coronado, T. J. Killeen, W. F. Laurance, C. Levis, W. E. Magnusson, B. S. Marimon, B. H. Marimon Junior, I. Mendoza Polo, P. Mishra, M. T. Nascimento, D. Neill, M. P. Núñez Vargas, W. A. Palacios, A. Parada, G. Pardo Molina, M. Peña-Claros, N. Pitman, C. A. Peres, L. Poorter, A. Prieto, H. Ramirez-Angulo, Z. Restrepo Correa, A. Roopsind, K. H. Roucoux, A. Rudas, R. P. Salomão, J. Schietti, M. Silveira, P. F. de Souza, M. K. Steininger, J. Stropp, J. Terborgh, R. Thomas, M. Toledo, A. Torres-Lezama, T. R. van Andel, G. M. F. van der Heijden, I. C. G. Vieira, S. Vieira, E. Vilanova-Torre, V. A. Vos, O. Wang, C. E. Zartman, Y. Malhi, O. L. Phillips, Markedly divergent estimates of Amazon forest carbon density from ground plots and satellites. *Global Ecology and Biogeography*. **23**, 935–946 (2014).

18. R. Dubayah, J. B. Blair, S. Goetz, L. Fatoyinbo, M. Hansen, S. Healey, M. Hofton, G. Hurtt, J. Kellner, S. Luthcke, J. Armston, H. Tang, L. Duncanson, S. Hancock, P. Jantz, S. Marselis, P. L. Patterson, W. Qi, C. Silva, The Global Ecosystem Dynamics Investigation: High-resolution laser ranging of the Earth's forests and topography. *Science of Remote Sensing*. **1**, 100002 (2020).

19. M. Réjou-Méchain, H. C. Muller-Landau, M. Detto, S. C. Thomas, T. Le Toan, S. S. Saatchi, J. S. Barreto-Silva, N. A. Bourg, S. Bunyavejchewin, N. Butt, W. Y. Brockelman, M. Cao, D. Cárdenas, J.-M. Chiang, G. B. Chuyong, K. Clay, R. Condit, H. S. Dattaraja, S. J. Davies, A. Duque, S. Esufali, C. Ewango, R. H. S. Fernando, C. D. Fletcher, I. A. U. N. Gunatilleke, Z. Hao, K. E. Harms, T. B. Hart, B. Hérault, R. W. Howe, S. P. Hubbell, D. J. Johnson, D. Kenfack, A. J. Larson, L. Lin, Y. Lin, J. A. Lutz, J.-R. Makana, Y. Malhi, T. R. Marthews, R. W. McEwan, S. M. McMahon, W. J. McShea, R. Muscarella, A. Nathalang, N. S. M. Noor, C. J. Nytch, A. A. Oliveira, R. P. Phillips, N. Pongpattananurak, R. Punchi-Manage, R. Salim, J. Schurman, R. Sukumar, H. S. Suresh, U. Suwanvecho, D. W. Thomas, J. Thompson, M. Uríarte, R. Valencia, A. Vicentini, A. T. Wolf, S. Yap, Z. Yuan, C. E. Zartman, J. K. Zimmerman, J. Chave, Local spatial structure of forest biomass and its consequences for remote sensing of carbon stocks. *Biogeosciences*. **11**, 6827–6840 (2014).

20. J. Esteban, R. E. McRoberts, A. Fernández-Landa, J. L. Tomé, E. Næsset, Estimating forest volume and biomass and their changes using random forests and remotely sensed data. *Remote Sensing*. **11**, 1944 (2019).

21. P. L. Patterson, S. P. Healey, G. Ståhl, S. Saarela, S. Holm, H. E. Andersen, R. O. Dubayah, L. Duncanson, S. Hancock, J. Armston, J. R. Kellner, W. B. Cohen, Z. Yang, Statistical properties of hybrid estimators proposed for GEDI - NASA's global ecosystem dynamics investigation. *Environmental Research Letters*. **14**, 065007 (2019).

22. Dubayah, Ralph, Hofton, Michelle, Blair, James, Armston, John, Tang, Hao, Luthcke, Scott, GEDI L2A Elevation and Height Metrics Data Global Footprint Level V002 (2021), , doi:10.5067/GEDI/GEDI02_A.002.

23. H. Tang, J. Armston, S. Hancock, S. Marselis, S. Goetz, R. Dubayah, Characterizing global forest canopy cover distribution using spaceborne lidar. *Remote Sensing of Environment*. **231** (2019), doi:10.1016/j.rse.2019.111262.

---

24. R. O. Dubayah, J. Armston, J. R. Kellner, L. Duncanson, S. P. Healey, P. L. Patterson, S. Hancock, H. Tang, J. Bruening, M. A. Hofton, J. B. Blair, S. B. Luthcke, GEDI L4A Footprint Level Aboveground Biomass Density, Version 2. *ORNL DAAC* (2021), doi:10.3334/ORNLDAAC/1986.

25. R. O. Dubayah, J. Armston, S. P. Healey, Z. Yang, P. L. Patterson, S. Saarela, G. Stahl, L. Duncanson, J. R. Kellner, GEDI L4B Gridded Aboveground Biomass Density (2022), , doi:10.3334/ORNLDAAC/2017.

26. G. Ståhl, S. Saarela, S. Schnell, S. Holm, J. Breidenbach, S. P. Healey, P. L. Patterson, S. Magnussen, E. Næsset, R. E. McRoberts, T. G. Gregoire, Use of models in large-area forest surveys: comparing model-assisted, model-based and hybrid estimation. *Forest Ecosystems*. **3**, 5 (2016).

27. T. G. Gregoire, Design-based and model-based inference in survey sampling: appreciating the difference. *Canadian Journal of Forest Research*. **28**, 1429–1447 (1998).

28. P. L. Patterson, S. P. Healey, G. Ståhl, S. Saarela, S. Holm, H.-E. Andersen, R. Dubayah, L. i Duncanson, S. Hancock, J. Armston, J. R. Kellner, W. B. Cohen, Z. Yang, Statistical properties of hybrid estimators proposed for GEDI – NASA's Global Ecosystem Dynamics Investigation. *Environmental Research Letters*. **14**, 65007 (2019).

29. T. G. Gregoire, G. Ståhl, E. Næsset, T. Gobakken, R. Nelson, S. Holm, Model-assisted estimation of biomass in a LiDAR sample survey in Hedmark county, Norway. *Canadian Journal of Forest Research*. **41**, 83–95 (2011).

30. J. Menlove, S. P. Healey, A Comprehensive Forest Biomass Dataset for the USA Allows Customized Validation of Remotely Sensed Biomass Estimates. *Remote Sensing*. **12** (2020), doi:10.3390/rs12244141.

31. J. C. Jenkins, D. C. Chojnacky, L. S. Heath, R. A. Birdsey, National-scale biomass estimators for United States tree species. *Forest Science*. **49**, 12–35 (2003).

32. R. E. McRoberts, E. Næsset, S. Saatchi, G. C. Liknes, B. F. Walters, Q. Chen, Local validation of global biomass maps. *International Journal of Applied Earth Observation and Geoinformation*. **83**, 101931 (2019).

33. V. Amrhein, S. Greenland, B. McShane, Scientists rise up against statistical significance. *Nature*. **567**, 305–307 (2019).

34. Natural Earth » 1:10m Cultural Vectors - Free vector and raster map data at 1:10m, 1:50m, and 1:110m scales, (available at https://www.naturalearthdata.com/downloads/10m-cultural-vectors/).

35. FAO, *Global Forest Resources Assessment 2020: Main report* (FAO, Rome, Italy, 2020; http://www.fao.org/documents/card/en/c/ca9825en).

36. L. Duncanson, J. Armston, M. Disney, V. Avitabile, N. Barbier, K. Calders, S. Carter, J. Chave, M. Herold, T. W. Crowther, M. Falkowski, J. R. Kellner, N. Labrière, R. Lucas, N. MacBean, R. E. McRoberts, V. Meyer, E. Næsset, J. E. Nickeson, K. I. Paul, O. L. Phillips, M. Réjou-Méchain, M. Román, S. Roxburgh, S. Saatchi, D. Schepaschenko, K. Scipal, P. R. Siqueira, A. Whitehurst, M. Williams, The Importance of Consistent Global Forest Aboveground Biomass Product Validation. *Surveys in Geophysics* (2019), doi:10.1007/s10712-019-09538-8.

37. A. J. Lister, C. T. Scott, S. Rasmussen, Inventory methods for trees in nonforest areas in the great plains states. *Environmental Monitoring and Assessment*. **184**, 2465–2474 (2012).

38. S. Schnell, D. Altrell, G. Ståhl, C. Kleinn, The contribution of trees outside forests to national tree biomass and carbon stocks—a comparative study across three continents. *Environmental Monitoring and Assessment*. **187**, 4197 (2014).

39. N. Thomas, P. Baltezar, D. Lagomasino, A. Stovall, Z. Iqbal, L. Fatoyinbo, Trees outside forests are an underestimated resource in a country with low forest cover. *Scientific Reports*. **11**, 7919 (2021).

40. L. Duncanson, J. R. Kellner, J. Armston, R. Dubayah, D. M. Minor, S. Hancock, S. P. Healey, P. L. Patterson, S. Saarela, S. Marselis, C. E. Silva, J. Bruening, S. J. Goetz, H. Tang, M. Hofton, B. Blair, S. Luthcke, L.

---

Fatoyinbo, K. Abernethy, A. Alonso, H.-E. Andersen, P. Aplin, T. R. Baker, N. Barbier, J. F. Bastin, P. Biber, P. Boeckx, J. Bogaert, L. Boschetti, P. B. Boucher, D. S. Boyd, D. F. R. P. Burslem, S. Calvo-Rodriguez, J. Chave, R. L. Chazdon, D. B. Clark, D. A. Clark, W. B. Cohen, D. A. Coomes, P. Corona, K. C. Cushman, M. E. J. Cutler, J. W. Dalling, M. Dalponte, J. Dash, S. de-Miguel, S. Deng, P. W. Ellis, B. Erasmus, P. A. Fekety, A. Fernandez-Landa, A. Ferraz, R. Fischer, A. G. Fisher, A. García-Abril, T. Gobakken, J. M. Hacker, M. Heurich, R. A. Hill, C. Hopkinson, H. Huang, S. P. Hubbell, A. T. Hudak, A. Huth, B. Imbach, K. J. Jeffery, M. Katoh, E. Kearsley, D. Kenfack, N. Kljun, N. Knapp, K. Král, M. Krůček, N. Labrière, S. L. Lewis, M. Longo, R. M. Lucas, R. Main, J. A. Manzanera, R. V. Martínez, R. Mathieu, H. Memiaghe, V. Meyer, A. M. Mendoza, A. Monerris, P. Montesano, F. Morsdorf, E. Næsset, L. Naidoo, R. Nilus, M. O'Brien, D. A. Orwig, K. Papathanassiou, G. Parker, C. Philipson, O. L. Phillips, J. Pisek, J. R. Poulsen, H. Pretzsch, C. Rüdiger, S. Saatchi, A. Sanchez-Azofeifa, N. Sanchez-Lopez, R. Scholes, C. A. Silva, M. Simard, A. Skidmore, K. Stereńczak, M. Tanase, C. Torresan, R. Valbuena, H. Verbeeck, T. Vrska, K. Wessels, J. C. White, L. J. T. White, E. Zahabu, C. Zgraggen, Aboveground biomass density models for NASA's Global Ecosystem Dynamics Investigation (GEDI) lidar mission. *Remote Sensing of Environment*. **270**, 112845 (2022).

41.  W. Ni, Z. Zhang, G. Sun, Assessment of Slope-Adaptive Metrics of GEDI Waveforms for Estimations of Forest Aboveground Biomass over Mountainous Areas. *Journal of Remote Sensing*. **2021** (2021), doi:10.34133/2021/9805364.

42.  N. Lang, N. Kalischek, J. Armston, K. Schindler, R. Dubayah, J. D. Wegner, Global canopy height regression and uncertainty estimation from GEDI LIDAR waveforms with deep ensembles. *Remote Sensing of Environment*. **268**, 112760 (2022).

43.  A. Burt, K. Calders, A. Cuni-Sanchez, J. Gómez-Dans, P. Lewis, S. L. Lewis, Y. Malhi, O. L. Phillips, M. Disney, Assessment of Bias in Pan-Tropical Biomass Predictions. *Frontiers in Forests and Global Change*. **3** (2020) (available at https://www.frontiersin.org/article/10.3389/ffgc.2020.00012).

44.  M. Disney, A. Burt, P. Wilkes, J. Armston, L. Duncanson, New 3D measurements of large redwood trees for biomass and structure. *Sci Rep*. **10**, 16721 (2020).

45.  Z. Wurtzebach, R. J. DeRose, R. R. Bush, S. A. Goeking, S. Healey, J. Menlove, K. A. Pelz, C. Schultz, J. D. Shaw, C. Witt, Supporting National Forest System Planning with Forest Inventory and Analysis Data. *Journal of Forestry*. **118**, 289–306 (2019).

46.  S. Saarela, S. Holm, S. P. Healey, H. E. Andersen, H. Petersson, W. Prentius, P. L. Patterson, E. Næsset, T. G. Gregoire, G. Ståhl, Generalized hierarchical model-based estimation for aboveground biomass assessment using GEDI and landsat data. *Remote Sensing* (2018), doi:10.3390/rs10111832.

47.  W. Qi, S. Saarela, J. Armston, G. Ståhl, R. Dubayah, Forest biomass estimation over three distinct forest types using TanDEM-X InSAR data and simulated GEDI lidar data. *Remote Sensing of Environment*. **232**, 111283 (2019).

48.  S. Saarela, S. Holm, S. P. Healey, P. L. Patterson, Z. Yang, H.-E. Andersen, R. O. Dubayah, W. Qi, L. Duncanson, J. Armston, A. A. Mensah, T. Gobakken, E. Naesset, M. Ekstrom, G. Stahl, Comparing methods for forest biomass assessment in connection with the GEDI mission. *Environmental Research Letters*. **10**, 1832 (2018).

49.  S. Saarela, S. Holm, A. Grafström, S. Schnell, E. Næsset, T. G. Gregoire, R. F. Nelson, G. Ståhl, Hierarchical model-based inference for forest inventory utilizing three sources of information. *Annals of Forest Science*. **73**, 895–910 (2016).

50.  G. Krieger, A. Moreira, H. Fiedler, I. Hajnsek, M. Werner, M. Younis, M. Zink, in *IEEE Transactions on Geoscience and Remote Sensing* (2007).

51.  P. Rosen, S. Hensley, S. Shaffer, W. Edelstein, Y. Kim, R. Kumar, T. Misra, R. Bhan, R. Satish, R. Sagi, in *2016 IEEE International Geoscience and Remote Sensing Symposium (IGARSS)* (2016), pp. 2106–2108.

52. K. Scipal, M. Arcioni, J. Chave, J. Dall, F. Fois, T. LeToan, C.-C. Lin, K. Papathanassiou, S. Quegan, F. Rocca, S. Saatchi, H. Shugart, L. Ulander, M. Williams, in *2010 IEEE International Geoscience and Remote Sensing Symposium* (2010), pp. 52–55.

53. S. Hancock, J. Armston, M. Hofton, X. Sun, H. Tang, L. I. Duncanson, J. R. Kellner, R. Dubayah, The GEDI Simulator: A Large-Footprint Waveform Lidar Simulator for Calibration and Validation of Spaceborne Missions. *Earth and Space Science*. **6**, 294–310 (2019).

54. M. Réjou-Méchain, H. C. Muller-Landau, M. Detto, S. C. Thomas, T. Le Toan, S. S. Saatchi, J. S. Barreto-Silva, N. A. Bourg, S. Bunyavejchewin, N. Butt, W. Y. Brockelman, M. Cao, D. Cárdenas, J. M. Chiang, G. B. Chuyong, K. Clay, R. Condit, H. S. Dattaraja, S. J. Davies, A. Duque, S. Esufali, C. Ewango, R. H. S. Fernando, C. D. Fletcher, I. A. U. N. Gunatilleke, Z. Hao, K. E. Harms, T. B. Hart, B. Hérault, R. W. Howe, S. P. Hubbell, D. J. Johnson, D. Kenfack, A. J. Larson, L. Lin, Y. Lin, J. A. Lutz, J. R. Makana, Y. Malhi, T. R. Marthews, R. W. Mcewan, S. M. Mcmahon, W. J. Mcshea, R. Muscarella, A. Nathalang, N. S. M. Noor, C. J. Nytch, A. A. Oliveira, R. P. Phillips, N. Pongpattananurak, R. Punchi-Manage, R. Salim, J. Schurman, R. Sukumar, H. S. Suresh, U. Suwanvecho, D. W. Thomas, J. Thompson, M. Uríarte, R. Valencia, A. Vicentini, A. T. Wolf, S. Yap, Z. Yuan, C. E. Zartman, J. K. Zimmerman, J. Chave, Local spatial structure of forest biomass and its consequences for remote sensing of carbon stocks. *Biogeosciences*. **11**, 6827–6840 (2014).

55. J. R. Kellner, J. Armston, L. Duncanson, Algorithm theoretical basis document for GEDI footprint aboveground biomass density (2021).

56. M. A. Friedl, D. Sulla-Menashe, B. Tan, A. Schneider, N. Ramankutty, A. Sibley, X. Huang, MODIS Collection 5 global land cover: Algorithm refinements and characterization of new datasets. *Remote Sensing of Environment*. **114**, 168–182 (2010).

57. M. A. Friedl, D. K. McIver, J. C. Hodges, X. Y. Zhang, D. Muchoney, A. H. Strahler, C. E. Woodcock, S. Gopal, A. Schneider, A. Cooper, Global land cover mapping from MODIS: algorithms and early results. *Remote sensing of Environment*. **83**, 287–302 (2002).

58. L. Duncanson, J. R. Kellner, J. Armston, R. O. Dubayah, Many other authors, Development of global lidar biomass density models for GEDI's L4A product. *Remote Sensing of Environment* (in review).

59. G. Ståhl, S. Holm, T. G. Gregoire, T. Gobakken, E. Næsset, R. Nelson, Model-based inference for biomass estimation in a LiDAR sample survey in Hedmark County, Norway. *Canadian Journal of Forest Research*. **41**, 96–107 (2011).

## Supplementary Materials

### Introduction
In these supplementary materials we present more details about the GEDI mission, describe how footprint-level biomass estimates are created that form the basis of gridded biomass estimates, and present the technical details of our statistical procedure that allows biomass estimates at the level of countries based on an efficient algorithm based on 6 km x 6 km tiles. These materials also include figures referenced in the main manuscript that provide additional insight into our results and two data tables that collect biomass results estimated globally by plant functional type and by country.

### The GEDI Mission
GEDI is led by the University of Maryland and NASA Goddard Spaceflight Center, in collaboration with the US Forest Service, Northern Arizona University and Brown University. GEDI began science collection on-board the ISS in April 2019. GEDI uses a laser altimeter comprised of 3 lasers to provide 8 transects of canopy structure observations along the Earth's surface. Each track is comprised of 25 m diameter footprints, with 60 m along track between footprints, and 600 m across track separating each of the transects. The ISS has orbital limit of 51.6° N&S and GEDI's observations are therefore constrained to fall within these latitudes. The ISS can be placed in either a repeating orbit or in a pseudo-random, precessing, and non-repeating orbit, dependent on altitude. In the first year of GEDI's mission, the ISS was in a precessing mode and GEDI's grouping of 8 ground tracks were randomly distributed across the Earth. During 2020 and 2021, the ISS was in an approximate 4-day, repeating orbit, which led to clustering of tracks on the surface, and the effects of which are visible in derived data products. As of 2022, changes in the ISS altitude have transitioned the platform away from 4-day repeats allowing GEDI to again achieve more uniform coverage.

The sole observable from GEDI is a return waveform which gives the vertical distribution of reflecting surfaces (e.g., leaves and branches) within the canopy, along with the underlying topographic elevation. Two of GEDI's three lasers are used in full-power mode with an approximate laser output of about 15 mJ, and the third laser is optically split into two beams. At any one instant four laser footprints illuminate the ground. The four tracks are then optoelectrically dithered across track every other shot, providing the 8 transects of data. Various metrics are derived from the waveform, including canopy height and canopy cover. These metrics are developed at the footprint (25 m) level.

### Footprint-Level Biomass Estimation
Modeling AGBD from waveform lidar metrics at the scale of GEDI footprints is well-established from studies of airborne laser scanning. These studies link field estimates of AGBD from plot data to waveform lidar metrics to develop predictive models that can be applied within regions. Because no globally comprehensive data set of paired lidar and AGBD existed prior to GEDI, footprint models were developed using simulated waveforms paired with ground-based field estimates of AGBD that are used to create the GEDI04_A product. Each simulated waveform was generated using discrete-return airborne lidar and the GEDI waveform simulator *(53)*. There are two advantages to using simulated waveforms to develop GEDI04_A models. One is that simulated waveforms reduce the impact of geolocation uncertainty *(54)*. A second advantage is that few locations are associated with field estimates of AGBD that could be used to train GEDI models. Because GEDI is a sampling mission and most field plots are small, GEDI data will not intersect most of these locations during the mission life.

The comprehensive training data set currently contains 31,414 simulated GEDI waveforms. Quality control filters were used to exclude some measurements from the version-1 GEDI04_A calibration data set. A detailed description of data filtering and quality control is in the GEDI04_A ATBD (*55*). After filtering and quality control, the database used to develop the version-1 GEDI04_A models contained 8,587 simulated GEDI waveforms in 21 countries.

Building globally representative GEDI04_A models requires stratification. The models are stratified by world region and an error-corrected and infilled version of MODIS Type 5 plant functional type (PFT) classification MCD12Q1 version 6 (*56, 57*). PFT classes are deciduous broadleaf trees (DBT; class 4), deciduous needleleaf trees (DNT; class 3), evergreen broadleaf trees (EBT, class 2), evergreen needleleaf trees (ENT, class 1), and grasses, shrubs, and woodlands (GSW, classes 5, 6, and 11). Two world regions are the geologically defined continents of Africa and Europe. The South America world region contains the Caribbean Islands, Central America and southern Mexico and the continent of South America. Australia, Papua New Guinea, and the islands on the east side of the Wallace line comprise the Australia and Oceania world region. The North America world region includes geological North America north of southern Mexico. The continent of Asia is divided into north and south regions that approximately correspond to temperate and tropical forests. Taken together, combinations of world region and PFT constitute 35 unique prediction strata within the GEDI domain (*58*).

GEDI04_A models must be transferable to new regions outside the limited extent of training data. To quantify geographic transferability during model development, candidate models were evaluated within sets of 5-degree grid cells that contain simulated GEDI waveforms with coincident field data. Data from one grid cell were held out, and models were trained on the remaining grid cells. Candidate models were used to predict AGBD within the held-out grid cell and the process was repeated for all grid cells in each prediction stratum and for all models under consideration (*58*). The performance of all candidate models was evaluated by ranking every model in order of smallest mean residual error, smallest percentage root mean squared error, the maximum RH metric in the model, the number of coefficients in the model, and the number of RH metrics in the model (*55*).

## Aggregating Tile-level Estimates to Larger Areas

The basic building blocks used in the procedure to estimate aboveground biomass at the level of countries, or larger areas, are 6×6 km tiles. Within these tiles models are applied to predict biomass for each of the GEDI footprints, following the hybrid inference methods described in Patterson et al. (*21*). As a result, the aboveground biomass density (AGBD) and the corresponding variance are estimated for each tile.

The tile level AGBD estimator under an unequal-size cluster (tracks with GEDI footprints) design, assuming the GEDI tracks to be randomly located, can be written as

$$\hat{\mu}_Y = \frac{\left(\sum_{i=1}^{m} \sum_{k=1}^{P_i} \sum_{t=1}^{T_{ik}} g_k(x_{ikt}, \widehat{\boldsymbol{\beta}}_k)\right)}{\sum_{i=1}^{m} T_i}, \tag{1}$$

where $m$ is the number of sampled GEDI clusters, $P_i$ is the number of models involved in the $i^{th}$ cluster, $T_{ik}$ is the number of GEDI footprints applying the $k^{th}$ model in cluster $i$, $x_{ikt}$ is the vector of GEDI variables, $g_k(x_{ikt}, \widehat{\boldsymbol{\beta}}_k)$ is predicted AGBD for the $t^{th}$ GEDI footprint in the $i^{th}$ cluster applying the $k^{th}$ model, and $T_i$ is the number of footprints in the $i^{th}$ cluster.

Formula (1) may be rewritten as (see Ståhl et al. (*59*) Eq. 11 and Patterson et al. (*21*), Eq. 3),

$$\hat{\mu}_Y = \frac{\sum_{i=1}^{m}\sum_{k=1}^{p_i}\sum_{t=1}^{T_{ik}} g_k(x_{ikt},\widetilde{\beta_k})}{\sum_{i=1}^{m} T_i} = \frac{\sum_{i=1}^{m}\hat{G}_i}{\sum_{i=1}^{m} T_i}, \tag{2}$$

where, $\hat{G}_i$ is the predicted AGBD total for the $i^{th}$ cluster.

Patterson et al. ($21$) applied the estimator from Ståhl et al. ($59$) (Eq. 11) for 1×1 km units where it is straightforward to assume that a single AGBD prediction model has been applied to all GEDI footprints. For larger building blocks, such as 6x6 km tiles, different models may have been applied to different footprints, since a tile may be divided between two or more ecoregions.

In developing a variance estimator for the estimator in Eq. 2, in case one or more models have been applied in a tile, we use the law of total variance, i.e.

$$V(\hat{\mu}_Y) = E_M[V_D(\hat{\mu}_Y)] + V_M(E_D[\hat{\mu}_Y]), \tag{3}$$

where $E_M[\cdot]$ and $E_D[\cdot]$ are expectations due to the model and design, respectively; and $V_M(\cdot)$ and $V_D(\cdot)$ are variances due to the model and design, respectively. First, we focus on the first term on the right-hand side of the expression. It is the model expectation of the design-based variance, i.e.,

$$E_M[V_D(\hat{\mu}_Y)] = V_D\left(\frac{\sum_{i=1}^{m} G_i}{\sum_{i=1}^{m} T_i}\right), \tag{4}$$

where, $G_i$ is the expected $i^{th}$ cluster total AGBD, according to the models. The estimator of $E_M[V_D(\hat{\mu}_Y)]$ follows Ståhl et al. ($59$) (Eq. 15, first term on the right-hand side),

$$\frac{1}{\bar{T}^2}\frac{\sum_{i=1}^{m}(\hat{G}_i - \hat{\mu}_Y T_i)^2}{m(m-1)}, \tag{5}$$

where $\bar{T}$ is a cluster average number of GEDI footprints. That is, this part remains unchanged, also if several models are applied when the cluster totals are computed.

The second term in (3) can be rewritten by rearranging the order of summation and excluding specific account for clusters since they are not important in the model-based part of the variance. We thus express it as

$$V_M(E_D[\hat{\mu}_Y]) = V_M\left(\frac{\sum_{k=1}^{P}\sum_{q=1}^{Q_k} g_k(x_{kq},\hat{\boldsymbol{\beta}}_k)}{N}\right), \tag{6}$$

where $P$ is the number of models employed in the tile, $Q_k$ is the number of units in the tile where the $k^{th}$ model should be applied and $N$ is the total number of units in the tile. The expression can be developed further into

$$V_M\left(\frac{\sum_{k=1}^{P}\sum_{q=1}^{Q_k} g_k(x_{kq},\hat{\boldsymbol{\beta}}_k)}{N}\right) = \frac{1}{N^2}\sum_{k=1}^{P}\left(\mathbf{1}_k^{*T}\widetilde{\boldsymbol{X}}_k^* Cov_k(\hat{\boldsymbol{\beta}}_k)\widetilde{\boldsymbol{X}}_k^{*T}\mathbf{1}_k^*\right) +$$
$$\frac{1}{N^2}\sum_{k=1}^{P}\sum_{l=1,k\neq l}^{P}\left(\mathbf{1}_k^{*T}\widetilde{\boldsymbol{X}}_k^* Cov_{kl}(\hat{\boldsymbol{\beta}}_k,\hat{\boldsymbol{\beta}}_l)\widetilde{\boldsymbol{X}}_l^{*T}\mathbf{1}_l^*\right), \tag{7}$$

where $\mathbf{1}_k^*$ is a $Q_k$-sized vector of units, $\widetilde{\boldsymbol{X}}_k^*$ is a matrix of partial derivatives with respect to the model parameters of the $k^{th}$ model; the size of the matrix is $Q_k$ × number of model parameters in the $k^{th}$ model, and $Cov_k(\hat{\boldsymbol{\beta}}_k)$ is the variance-covariance matrix of the estimated model parameters for the $k^{th}$ model. Since the different models were developed independently all cross-covariances between parameters from different models are zero, i.e., the covariance $Cov_{kl}(\hat{\boldsymbol{\beta}}_k,\hat{\boldsymbol{\beta}}_l) = 0$. Thus,

$$V_M \left( \frac{\sum_{k=1}^{P} \sum_{q=1}^{Q_k} g_k(x_{kq}, \widehat{\boldsymbol{\beta}}_k)}{N} \right) = \frac{1}{N^2} \sum_{k=1}^{P} \left( \mathbf{1}_k^{*T} \widetilde{\boldsymbol{X}}_k^* Cov_k(\widehat{\boldsymbol{\beta}}_k) \widetilde{\boldsymbol{X}}_k^{*T} \mathbf{1}_k^* \right) \tag{8}$$

For the variance estimator, $Cov_k(\widehat{\boldsymbol{\beta}}_k)$ is replaced by its estimator, and $\frac{Q_k}{N}$ is replaced by the corresponding sampling fraction. The variance estimator due to the modelling is then

$$\frac{1}{n^2} \sum_{k=1}^{P} \left( \mathbf{1}_k^T \widetilde{\boldsymbol{X}}_k \widehat{Cov}_k(\widehat{\boldsymbol{\beta}}_k) \widetilde{\boldsymbol{X}}_k^T \mathbf{1}_k \right), \tag{9}$$

where $n$ is the number of sampled GEDI footprints and $\mathbf{1}_k$ and $\widetilde{\boldsymbol{X}}_k$ are taken over sampled GEDI footprints.

Thus, the variance estimator is

$$\hat{V}(\hat{\mu}_Y) = \frac{1}{\bar{T}^2} \frac{\sum_{i=1}^{m} (\hat{G}_i - \hat{\mu}_Y T_i)^2}{m(m-1)} + \frac{1}{n^2} \sum_{k=1}^{P} \left( \mathbf{1}_k^T \widetilde{\boldsymbol{X}}_k \widehat{Cov}_k(\widehat{\boldsymbol{\beta}}_k) \widetilde{\boldsymbol{X}}_k^T \mathbf{1}_k \right). \tag{10}$$

In estimating AGBD across larger areas, such as countries, the tile-level AGBD estimates need to be aggregated and averaged. The AGBD estimate for a larger area of interest thus is

$$\hat{\mu}_{AOI} = \sum_{h=1}^{H} W_h \, \hat{\mu}_{Y_h}, \tag{11}$$

where $H$ is the number of tiles involved, $W_h = \frac{N_h}{\sum_{h=1}^{H} N_h}$ is the tile weight of the $h^{th}$ tile (in case the tiles are not equally large), $N_h$ is the number of units in the tile, and $\hat{\mu}_{Y_h}$ is the estimated AGBD in the tile.

In developing a variance estimator, it should be observed that the tile-level estimators typically are dependent since (i) the same models have been applied in several tiles and (ii) the GEDI tracks extend across several tiles and thus potentially cause correlated sampling errors.
A generic variance estimator for this case is given in Ståhl et al. (*59*) (Eq. 14). Employing our notation, the variance estimator can be rewritten as

$$\hat{V}(\hat{\mu}_{AOI}) = \sum_{h=1}^{H} W_h^2 \hat{V}_h(\hat{\mu}_{Y_h}) + \sum_{h=1}^{H} \sum_{r=1, h \neq r}^{H} \frac{W_h}{\bar{T}_h} \frac{W_r}{\bar{T}_r} \frac{\sum_{i=1}^{m_{hr}^*} (\hat{G}_{i_h} - \hat{\mu}_{Y_h} T_{i_h})(\hat{G}_{i_r} - \hat{\mu}_{Y_r} T_{i_r})}{m_{hr}^*(m_{hr}^* - 1)} +$$
$$\sum_{h=1}^{H} \sum_{r=1, h \neq r}^{H} \frac{W_h}{n_h} \frac{W_r}{n_r} \sum_{k=1}^{P_{hr}^*} (\mathbf{1}_{k_h}^T \widetilde{\boldsymbol{X}}_{k_h} \widehat{Cov}_k(\widehat{\boldsymbol{\beta}}_k) \widetilde{\boldsymbol{X}}_{k_r}^T \mathbf{1}_{k_r}). \tag{12}$$

The variance estimator (Eq. 12) has three terms on the right-hand side. The first term is just a weighted sum of estimated tile-level variances, i.e.

$$\sum_{h=1}^{H} W_h^2 \hat{V}_h(\hat{\mu}_{Y_h}) = \sum_{h=1}^{H} W_h^2 \left( \frac{1}{\bar{T}_h^2} \frac{\sum_{i=1}^{m_h} (\hat{G}_{i_h} - \hat{\mu}_{Y_h} T_{i_h})^2}{m_h(m_h - 1)} \right) +$$
$$\sum_{h=1}^{H} W_h^2 \left( \frac{1}{n_h^2} \sum_{k=1}^{P_h} (\mathbf{1}_{k_h}^T \widetilde{\boldsymbol{X}}_{k_h} \widehat{Cov}_k(\widehat{\boldsymbol{\beta}}_k) \widetilde{\boldsymbol{X}}_{k_h}^T \mathbf{1}_{k_h}) \right). \tag{13}$$

The second term in (12) is the sum of covariances because a GEDI track can cross several tiles, and hence, there is a dependency between clusters across tiles:

$$\sum_{h=1}^{H} \sum_{r=1, h \neq r}^{H} \frac{W_h}{\bar{T}_h} \frac{W_r}{\bar{T}_r} \frac{\sum_{i=1}^{m_{hr}^*} (\hat{G}_{i_h} - \hat{\mu}_{Y_h} T_{i_h})(\hat{G}_{i_r} - \hat{\mu}_{Y_r} T_{i_r})}{m_{hr}^*(m_{hr}^* - 1)}. \tag{14}$$

Here, $m_{hr}^*$ is the number of union clusters of tiles $h$ and $r$ e.g., $m_{hr}^* = 5 + 10 - 3 = 12$, if the $h^{th}$ tile has 5 clusters and the $r^{th}$ tile has 10, and 3 clusters cross each of tiles $h$ and $r$. However, numerically, the sum $\sum_{i=1}^{m_{hr}^*} (\hat{G}_{i_h} - \hat{\mu}_{Y_h} T_{i_h})(\hat{G}_{i_r} - \hat{\mu}_{Y_r} T_{i_r})$ should only be computed over those clusters, which cross both tile $h$ and $r$, because for the other pairs the product $(\hat{G}_{i_h} - \hat{\mu}_{Y_h} T_{i_h})(\hat{G}_{i_r} - \hat{\mu}_{Y_r} T_{i_r})$ should be zero due to independency between clusters. In our example, the numerator is a sum over 3 common clusters and the denominator is $12 \times (12 - 1)$.

The third term in (12) is the sum of covariances because a given model can be applied across several tiles. Hence, there is a dependency due to the modelling between tiles:

$$\sum_{h=1}^{H} \sum_{r=1, h \neq r}^{H} \frac{W_h}{n_h} \frac{W_r}{n_r} \sum_{k=1}^{P_{hr}^*} (\mathbf{1}_{k_h}^T \tilde{\mathbf{X}}_{k_h} \widehat{Cov}_k(\hat{\boldsymbol{\beta}}_k) \tilde{\mathbf{X}}_{k_r}^T \mathbf{1}_{k_r}). \tag{15}$$

Here, $P_{hr}^*$ is the intersection of models used in tiles $h$ and $r$. For example, if 3 models are employed to predict AGBD in tile $h$ and 2 models in tile $r$, but only 1 model is common to both tiles, then $P_{hr}^* = 1$.

Thus, Eq. (12) provides a AGBD variance estimator when tiles are aggregated to obtain AGBD estimators for larger areas; the details of the components are explained in Eqs. 13-15. However, the computational burden related to computing the variance components presented in Eqs. 14-15 may be challenging when aggregation is made across a large number of tiles. Thus, for computational reasons further simplification is motivated.

First, it should be observed that sampling covariance according to Eq. (14) would only occur for units that are located close to each other geographically. For units separated by great distances, the covariance should be approximately zero. In practice this means that this component only needs to be computed for pairs of units that are located relatively close to each other and be assigned to zero for other pairs. In this paper, we ignore sampling dependencies beyond the scale of 72 km tiles.

For the model covariances in Eq. (15) another approach to simplification must be adopted since covariances exist also across great geographical distances if the same models have been applied. To address this, we merge Eq. (15) with the second term on the right-hand side of Eq. (13) to

$$\sum_{h=1}^{H} \sum_{r=1}^{H} \frac{W_h}{n_h} \frac{W_r}{n_r} \sum_{k=1}^{P_{hr}^*} (\mathbf{1}_{k_h}^T \tilde{\mathbf{X}}_{k_h} \widehat{Cov}_k(\hat{\boldsymbol{\beta}}_k) \tilde{\mathbf{X}}_{k_r}^T \mathbf{1}_{k_r}), \tag{16}$$

i.e., the double sum now also includes diagonal elements. The expression can be further developed into

$$\sum_{h=1}^{H} \sum_{r=1}^{H} \frac{W_h}{n_h} \frac{W_r}{n_r} \sum_{k=1}^{P_{hr}^*} \sum_{i=1}^{q_k} \sum_{j=1}^{q_k} \left( t_{h_{k_i}} \widehat{Cov}_k \left( \hat{\beta}_{k_i}, \hat{\beta}_{k_j} \right) t_{r_{k_j}} \right), \tag{17}$$

where $q_k$ is the number of model parameters in the $k^{th}$ model, $t_{h_{k_i}}$ is the sum of partial derivatives for the $i^{th}$ model parameter in the $k^{th}$ model for the $h^{th}$ tile, $t_{r_{k_j}}$ is the sum of partial derivatives for the $j^{th}$ model parameter in the $k^{th}$ model for the $r^{th}$ tile, and $\widehat{Cov}_k \left( \hat{\beta}_{k_i}, \hat{\beta}_{k_j} \right)$ is the estimated covariance between the $i^{th}$ and $j^{th}$ model parameters in model $k$.

By rearranging the order of summation, summing over all models, but only for those tiles where a given model is applied, the expression can be rewritten as

$$\sum_{k=1}^{P} \sum_{i=1}^{q_k} \sum_{j=1}^{q_k} \sum_{h=1}^{H_k} \sum_{r=1}^{H_k} \left( \frac{W_h}{n_h} t_{h_{k_i}} \widehat{Cov}_k \left( \hat{\beta}_{k_i}, \hat{\beta}_{k_j} \right) t_{r_{k_j}} \frac{W_r}{n_r} \right), \tag{18}$$

where $P$ is the total number of models used in the area of interest and $H_k$ is the number of tiles where the $k^{th}$ model is applied. Since the estimated model parameter covariances do not depend on tiles, they can be moved outside the tile-related double summation, i.e.

$$\sum_{k=1}^{P} \sum_{i=1}^{q_k} \sum_{j=1}^{q_k} \widehat{Cov}_k \left( \hat{\beta}_{k_i}, \hat{\beta}_{k_j} \right) \sum_{h=1}^{H_k} \sum_{r=1}^{H_k} \left( \frac{W_h}{n_h} t_{h_{k_i}} \frac{W_r}{n_r} t_{r_{k_j}} \right). \tag{19}$$

This expression can be further developed as

$$\sum_{k=1}^{P} \sum_{k=1}^{q_k} \sum_{j=1}^{q_k} \widehat{Cov}_k \left( \hat{\beta}_{k_i}, \hat{\beta}_{k_j} \right) \sum_{h=1}^{H_k} \frac{W_h}{n_h} t_{h_{k_i}} \sum_{r=1}^{H_k} \frac{W_r}{n_r} t_{r_{k_i}}. \tag{20}$$

and finally simplified to

$$\sum_{k=1}^{P} \sum_{k=1}^{q_k} \sum_{j=1}^{q_k} \widehat{Cov}_k \left( \hat{\beta}_{k_i}, \hat{\beta}_{k_j} \right) T_{k_i} T_{k_j}, \tag{21}$$

where $T_{k_i}$ is a weighted sum of partial derivatives for the $i^{th}$ model parameter in the $k^{th}$ model across the $H_k$ tiles (i.e., the tiles where the $k^{th}$ model is applied), and $T_{k_j}$ is the corresponding weighted sum for the $j^{th}$ model parameter.

Although Eq. (21) involves a triple sum, its dimension typically is very small and thus the computational burden involved in estimating it is limited compared to applying Eq. 16 (or Eq. 15). Thus, the computationally more efficient version of the variance estimator for aggregated tile-based AGBD estimates is

$$\hat{V}(\hat{\mu}_{AOI}) = \sum_{h=1}^{H} W_h^2 \left( \frac{1}{\bar{T}_h^2} \frac{\sum_{i=1}^{m_h} \left( \hat{G}_{i_h} - \hat{\mu}_{Y_h} T_{i_h} \right)^2}{m_h(m_h-1)} \right) + \sum_{h=1}^{H} \sum_{r=1, h \neq r}^{H} \frac{W_h}{\bar{T}_h} \frac{W_r}{\bar{T}_r} \frac{\sum_{i=1}^{m_{hr}^*} \left( \hat{G}_{i_h} - \hat{\mu}_{Y_h} T_{i_h} \right)\left( \hat{G}_{i_r} - \hat{\mu}_{Y_r} T_{i_r} \right)}{m_{hr}^*(m_{hr}^*-1)} +$$
$$\sum_{k=1}^{P} \sum_{k=1}^{q_k} \sum_{j=1}^{q_k} \widehat{Cov}_k \left( \hat{\beta}_{k_i}, \hat{\beta}_{k_j} \right) T_{k_i} T_{k_j} \tag{22}$$

The estimators in Eq. (12) and Eq. (22) result in identical estimates, but Eq. (22) eases the computational burden.

# References

References in the Supplemental Materials appear in the reference list of the main text.

# Supplementary Figures
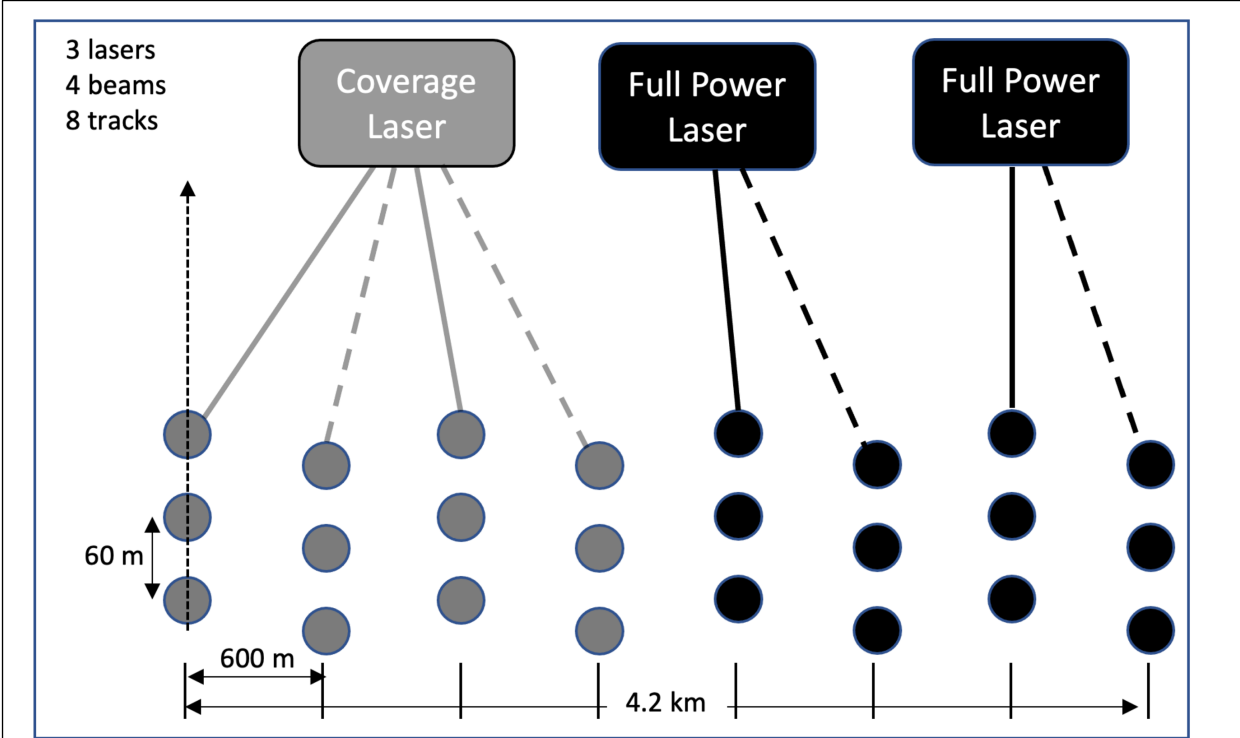


**Fig. S1.** **The GEDI beam pattern.** GEDI uses three lasers to produce 4 beams of 25 m diameter. The Coverage Laser output is split into two beams. Each of these beams are dithered across the ISS orbital track to produce 8 transects or tracks of data, where each footprint is separated by 60 m along-track and 600 m across track. Returned waveforms from each footprint are used to derive vertical canopy structure, such as height, as inputs to calibration equations that then predict aboveground biomass density for that footprint.
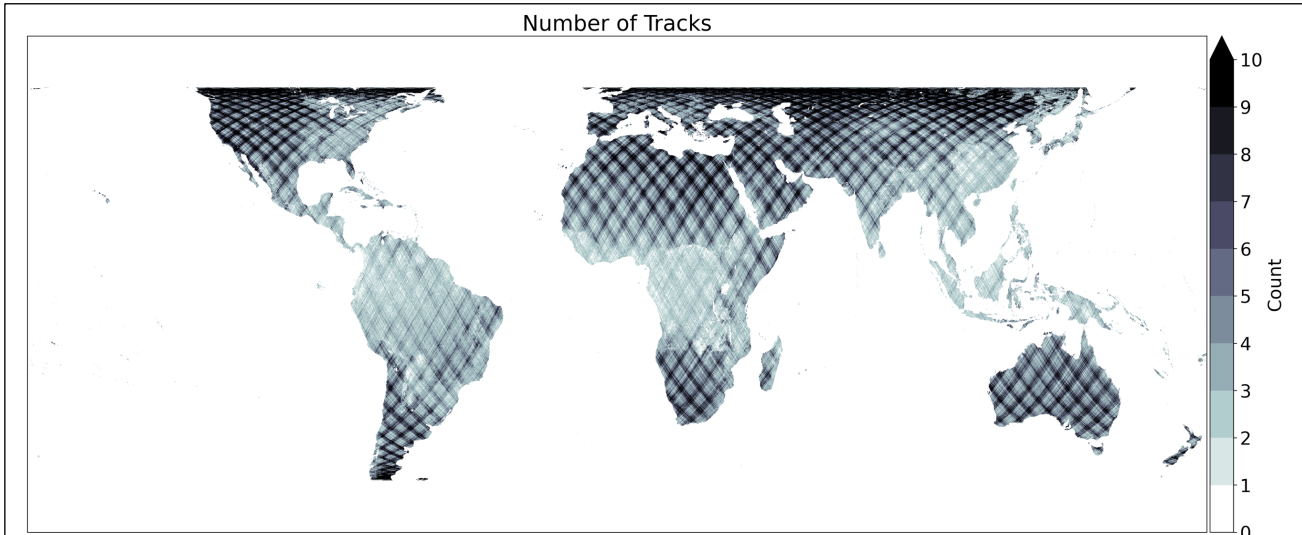
**Fig. S2**. **GEDI orbital coverage.** The number of GEDI laser tracks within 1 km cells is shown for the period from April 2019 to August 2021. During 2019 the ISS was in a randomly precessing orbit that provided relatively uniform coverage by longitude (represented by the light blue colors in the background). Beginning in early 2020, a change in the ISS orbital altitude placed it in a near 4-day repeating orbiting, providing high density coverage of GEDI shots for cells near the ISS ground tracks, but low coverage away from them, resulting in the strong diagonal patterns shown. Separately from this issue, coverage is always denser near the limits of the orbital inclination of the ISS (51.6° N&S), as the ground tracks converge and results in nearly continuous coverage across the land surface as these latitudinal limits are approached. The ISS orbit was subsequently lowered in 2022 resulting in more uniform coverage.
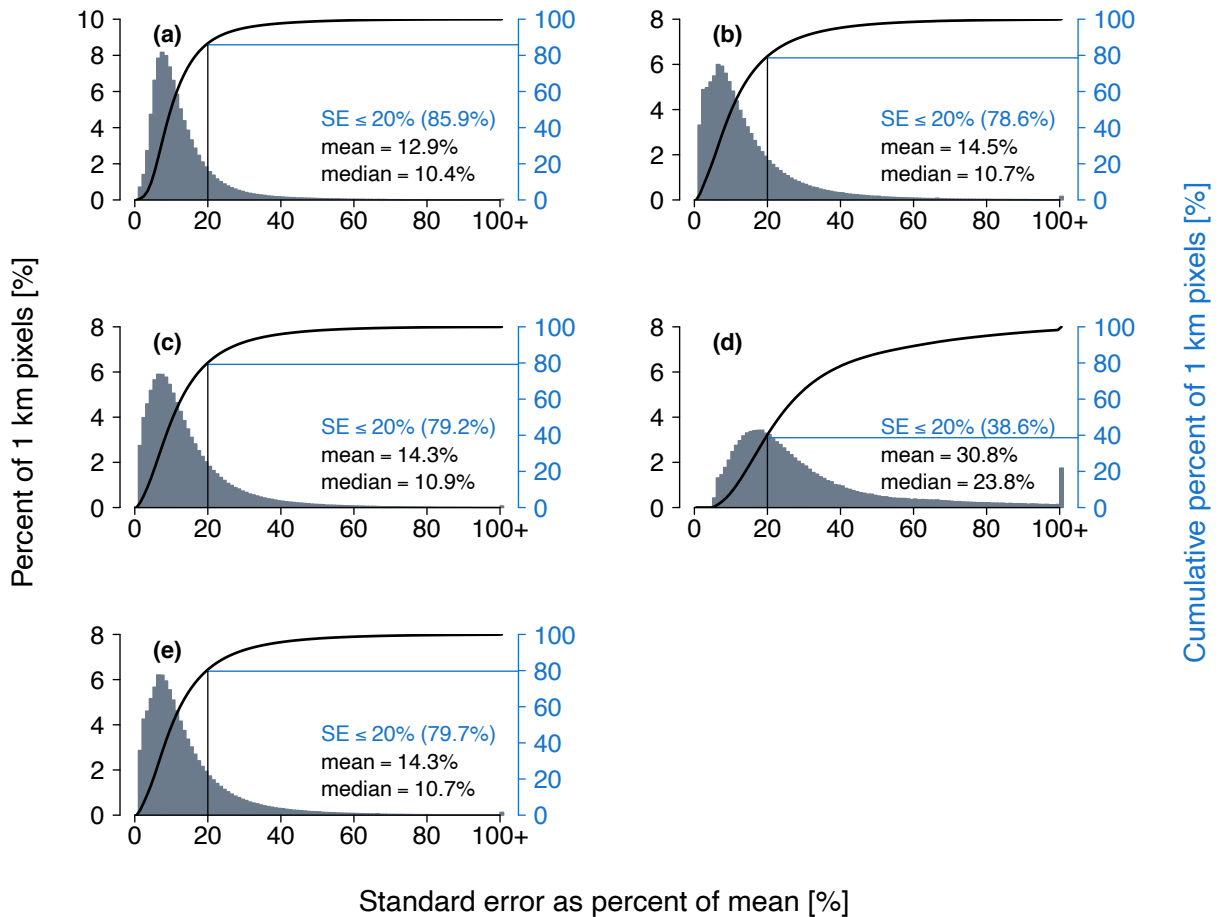
**Fig. S3. Biomass standard errors for high biomass cells by PFT.** Plots show errors for 1 km cells whose mean biomass is > 100 Mg/ha. Black line gives cumulative percentages. Blue horizontal lines give the cumulative percent of cells with standard errors ≤ 20%. **(a)** Needleleaf **(b)** Evergreen broadleaf **(c)** Deciduous broadleaf **(d)** Grass-shrub-woodland **(e)** Forested (all PFTs except Grass-shrub-woodland).
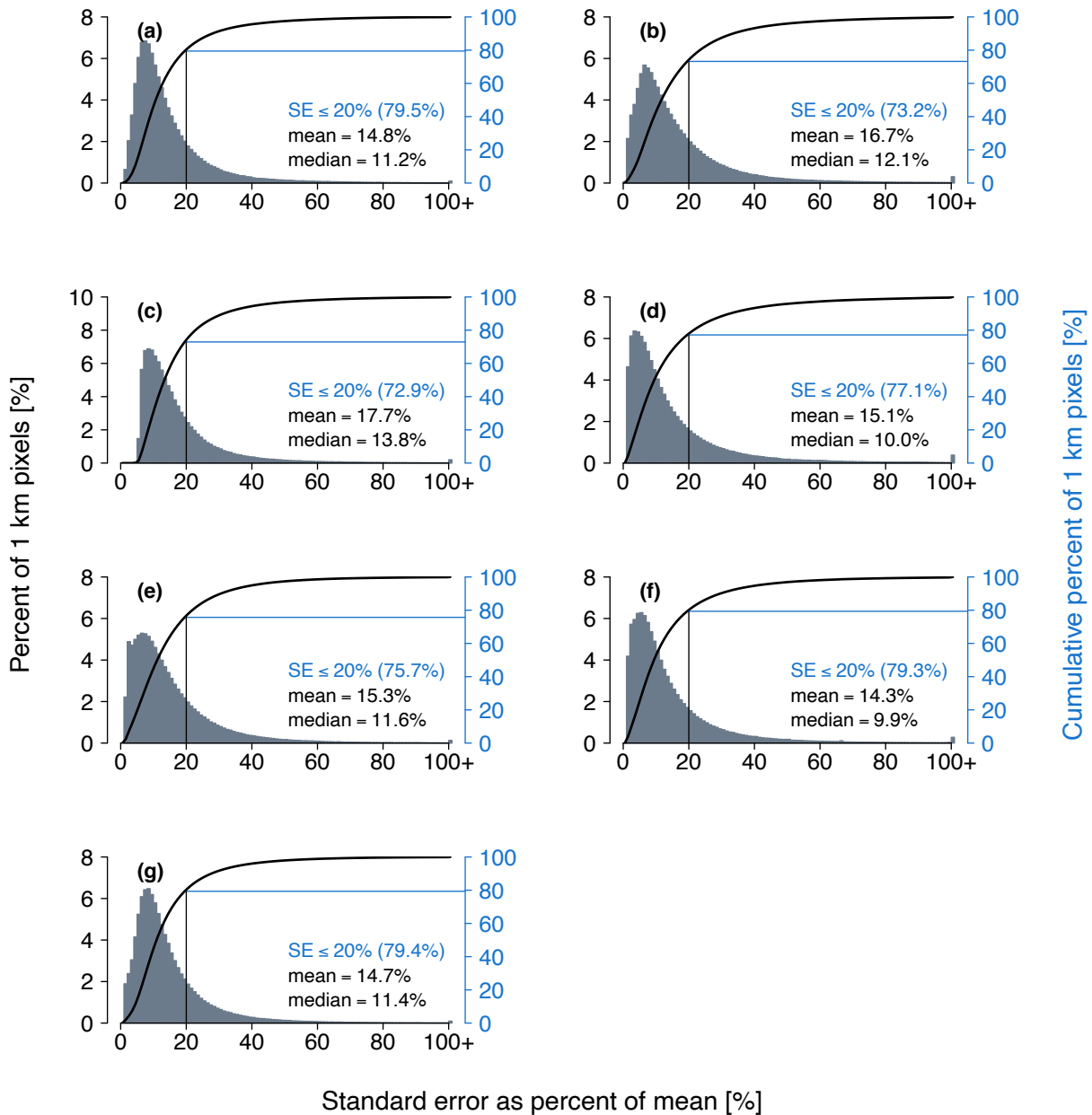
**Fig. S4. Biomass standard errors for high biomass cells by region.** Plots show errors for 1 km cells whose mean biomass is > 100 Mg/ha. Black line gives cumulative percentages. Blue horizontal lines give the cumulative percent of cells with standard errors ≤ 20%. **(a)** Europe **(b)** North Asia **(c)** Australasia **(d)** Africa **(e)** South Asia **(f)** South America **(g)** North America.

**Fig. S5**. **Relationship between GEDI and FAO AGBD.** Solid line is 1:1; slope and $R^2$ are found from linear regression between the two variables. RMSD (root mean square difference) is found using the difference between GEDI and FAO estimates. Data for each country is given in Table S2.
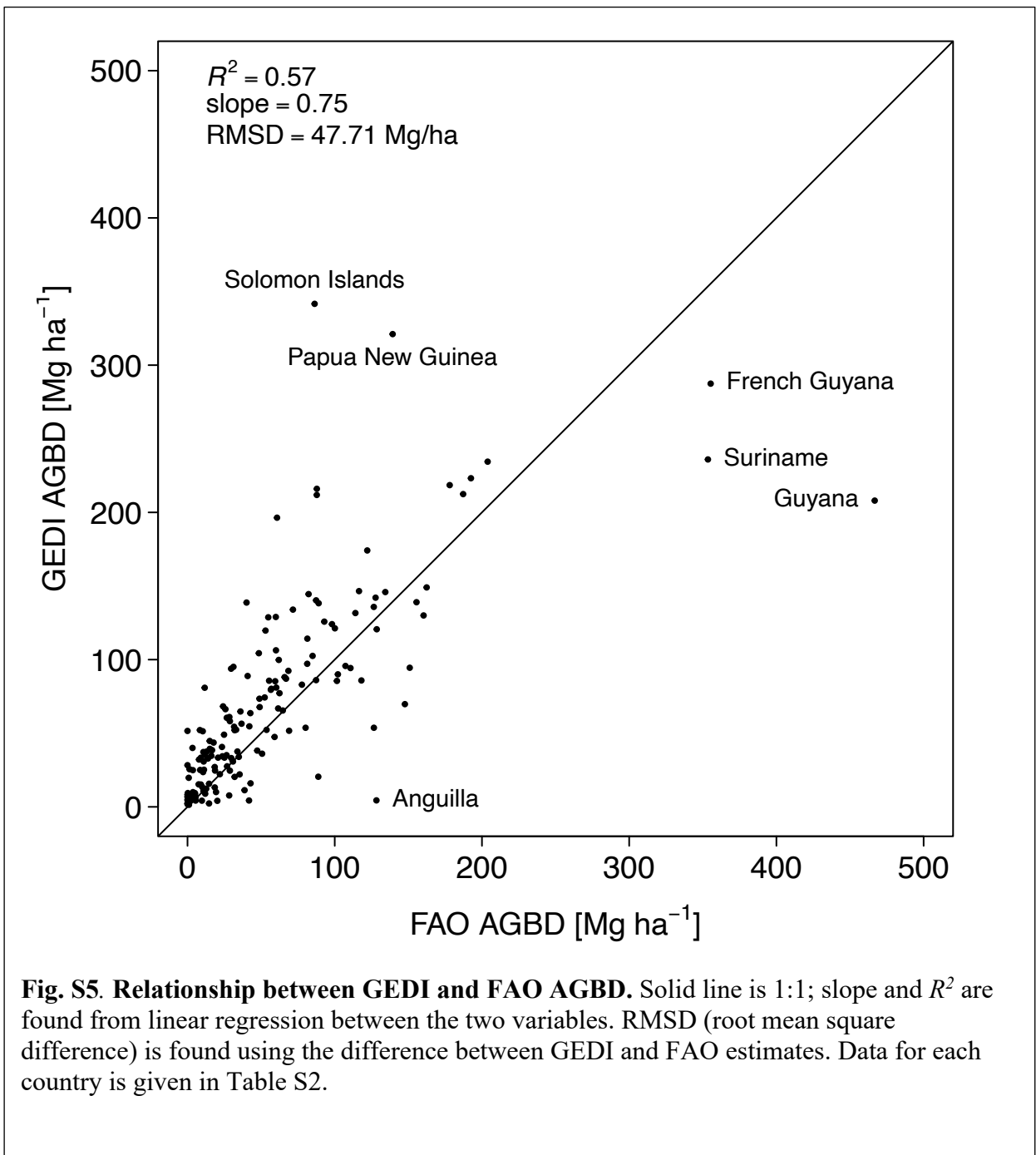
# Supplementary Tables

**Table S1.  Aboveground biomass densities (AGBD).** GEDI estimated AGBD by plant functional type (PFT) and by *PFT x region*.

| Name | Global Area [%] | PFT Area [%] | Region Area [%] | AGBD mean [Mg ha-1] | AGBD standard deviation [Mg ha-1] | Among all land cells, percent that meet requirements | Among land cells where GEDI makes an estimate, percent that meet requirements |
|---|---|---|---|---|---|---|---|
| Global | 100.000 | 100.000 | 100.000 | 35.890 | 69.763 | 70.451 | 94.841 |
| NT | 3.310 | 100.000 | 3.312 | 92.778 | 78.290 | 83.030 | 92.316 |
| EBT | 21.362 | 100.000 | 21.374 | 126.727 | 115.148 | 42.273 | 82.509 |
| DBT | 12.118 | 100.000 | 12.126 | 81.229 | 68.525 | 38.137 | 86.772 |
| GSW | 52.480 | 100.000 | 52.511 | 9.500 | 22.051 | 86.569 | 98.238 |
| FORESTED | 36.791 | 100.000 | 36.813 | 108.886 | 101.091 | 44.578 | 85.206 |
| Europe | 4.169 | 4.169 | 100.000 | 49.102 | 54.894 | 85.099 | 93.623 |
| North Asia | 20.190 | 20.190 | 100.000 | 21.984 | 46.625 | 83.359 | 96.309 |
| Australia | 8.970 | 8.970 | 100.000 | 37.915 | 97.235 | 81.887 | 95.795 |
| Africa | 28.348 | 28.348 | 100.000 | 17.363 | 44.010 | 68.615 | 97.844 |
| South Asia | 9.391 | 9.391 | 100.000 | 62.900 | 85.760 | 49.191 | 90.139 |
| South America | 17.606 | 17.606 | 100.000 | 65.025 | 95.025 | 56.594 | 90.173 |
| North America | 11.267 | 11.267 | 100.000 | 45.116 | 64.618 | 76.788 | 93.503 |
| NT Europe | 0.445 | 13.422 | 10.665 | 95.500 | 59.539 | 89.969 | 94.262 |
| NT North Asia | 0.703 | 21.236 | 3.484 | 123.569 | 78.585 | 68.671 | 87.745 |
| NT Australia | 0.087 | 2.639 | 0.974 | 100.812 | 52.038 | 76.952 | 86.292 |
| NT Africa | 0.024 | 0.729 | 0.085 | 48.137 | 34.139 | 83.132 | 95.035 |
| NT South Asia | 0.165 | 4.982 | 1.757 | 80.948 | 71.228 | 58.123 | 90.412 |
| NT South America | 0.150 | 4.542 | 0.854 | 102.684 | 88.990 | 71.039 | 83.854 |
| NT North America | 1.735 | 52.396 | 15.404 | 82.121 | 80.318 | 90.784 | 94.342 |
| EBT Europe | 0.164 | 0.770 | 3.945 | 55.896 | 32.954 | 88.758 | 94.468 |
| EBT North Asia | 0.186 | 0.869 | 0.919 | 167.649 | 101.561 | 57.644 | 84.974 |
| EBT Australia | 2.244 | 10.502 | 25.014 | 156.049 | 167.966 | 56.445 | 82.428 |
| EBT Africa | 4.416 | 20.668 | 15.577 | 112.012 | 93.063 | 33.081 | 84.592 |
| EBT South Asia | 4.376 | 20.480 | 46.594 | 130.687 | 99.813 | 35.264 | 78.474 |
| EBT South America | 9.563 | 44.760 | 54.317 | 124.142 | 108.856 | 44.055 | 82.540 |
| EBT North America | 0.413 | 1.935 | 3.670 | 101.173 | 83.613 | 71.129 | 88.993 |
| DBT Europe | 1.026 | 8.466 | 24.615 | 107.082 | 59.169 | 62.549 | 82.241 |
| DBT North Asia | 1.662 | 13.712 | 8.231 | 122.173 | 74.028 | 39.869 | 84.841 |
| DBT Australia | 0.001 | 0.004 | 0.006 | 17.712 | 35.354 | 32.982 | 93.532 |
| DBT Africa | 3.710 | 30.608 | 13.086 | 44.728 | 40.966 | 27.512 | 94.055 |
| DBT South Asia | 0.866 | 7.148 | 9.225 | 77.097 | 48.140 | 26.734 | 88.671 |

| | | | | | | | |
|---|---|---|---|---|---|---|---|
| **DBT South America** | **1.858** | **15.326** | **10.551** | **12.647** | **26.512** | **40.866** | **97.574** |
| **DBT North America** | 2.996 | 24.723 | 26.595 | 106.777 | 65.385 | 43.575 | 79.604 |
| **GSW Europe** | 0.822 | 1.564 | 19.714 | 18.315 | 34.855 | 89.593 | 94.749 |
| **GSW North Asia** | 15.779 | 30.038 | 78.152 | 12.088 | 26.928 | 88.641 | 97.241 |
| **GSW Australia** | 6.359 | 12.106 | 70.894 | 7.120 | 15.403 | 90.775 | 99.340 |
| **GSW Africa** | 18.945 | 36.065 | 66.828 | 5.742 | 13.340 | 84.636 | 99.466 |
| **GSW South Asia** | 1.101 | 2.097 | 11.729 | 13.028 | 25.467 | 77.900 | 97.302 |
| **GSW South America** | 5.201 | 9.900 | 29.538 | 13.311 | 27.650 | 81.013 | 96.727 |
| **GSW North America** | 4.273 | 8.135 | 37.928 | 12.212 | 24.984 | 89.640 | 97.788 |
| **FORESTED Europe** | 1.635 | 4.444 | 39.225 | 97.648 | 59.083 | 72.640 | 87.384 |
| **FORESTED North Asia** | 2.551 | 6.932 | 12.634 | 126.628 | 79.498 | 49.104 | 85.949 |
| **FORESTED Australia** | 2.332 | 6.337 | 25.995 | 153.366 | 164.683 | 57.208 | 82.616 |
| **FORESTED Africa** | 8.150 | 22.147 | 28.748 | 85.765 | 83.701 | 30.694 | 88.294 |
| **FORESTED South Asia** | 5.407 | 14.694 | 57.576 | 122.428 | 96.179 | 34.595 | 80.158 |
| **FORESTED South America** | 11.571 | 31.446 | 65.722 | 109.254 | 108.261 | 43.894 | 84.514 |
| **FORESTED North America** | 5.145 | 13.983 | 45.669 | 94.958 | 75.245 | 61.712 | 87.216 |

**Table S2. Country-level biomass estimates**. GEDI and FAO estimates of mean aboveground biomass (AGB), density (AGBD) and standard errors (SE) of the mean.

| Country | Percent Forest [%] | FAO Forested AGBD [Mg ha⁻¹] | FAO Total AGBD [Mg ha⁻¹] | GEDI Total AGBD [Mg ha⁻¹] | GEDI AGBD SE [Mg ha-1] | GEDI AGBD SE [%] | FAO AGB [Pg] | GEDI AGB [Pg] | GEDI AGB SE [Pg] |
|---|---|---|---|---|---|---|---|---|---|
| Afghanistan | 1.851 | NA | NA | 24.665 | 1.321 | 5.358 | NA | 1.584E+00 | 8.486E-02 |
| Åland | NA | NA | NA | NA | NA | NA | NA | NA | NA |
| Albania | 28.792 | NA | NA | 56.874 | 1.421 | 2.498 | NA | 1.612E-01 | 4.026E-03 |
| Algeria | 0.818 | 29.390 | 0.241 | 3.864 | 0.548 | 14.171 | 5.728E-02 | 8.921E-01 | 1.264E-01 |
| Andorra | 34.043 | 154.000 | 52.426 | 74.302 | 4.684 | 6.303 | 2.464E-03 | 3.360E-03 | 2.118E-04 |
| Angola | 53.427 | 30.300 | 16.188 | 34.647 | 0.645 | 1.862 | 2.018E+00 | 4.312E+00 | 8.028E-02 |
| Anguilla | 61.111 | 210.000 | 128.333 | 4.392 | 0.988 | 22.501 | 1.155E-03 | 3.544E-05 | 7.973E-06 |
| Antigua and Barbuda | 18.455 | 210.000 | 38.755 | 11.306 | 1.513 | 13.378 | 1.705E-03 | 5.105E-04 | 6.829E-05 |
| Argentina | 10.441 | 185.740 | 19.393 | 10.041 | 0.481 | 4.789 | 5.307E+00 | 2.796E+00 | 1.339E-01 |
| Armenia | 11.537 | NA | NA | 29.318 | 1.201 | 4.096 | NA | 8.675E-02 | 3.553E-03 |
| Aruba | 2.333 | NA | NA | 2.094 | 0.494 | 23.600 | NA | 3.554E-05 | 8.388E-06 |
| Ashmore and Cartier Islands | NA | NA | NA | NA | NA | NA | NA | NA | NA |
| Australia | 17.443 | 83.980 | 14.649 | 15.686 | 0.792 | 5.048 | 1.125E+01 | 1.206E+01 | 6.090E-01 |
| Austria | 47.251 | 172.300 | 81.413 | 114.239 | 2.179 | 1.907 | 6.718E-01 | 9.595E-01 | 1.830E-02 |
| Azerbaijan | 13.692 | NA | NA | 29.509 | 0.977 | 3.309 | NA | 2.545E-01 | 8.423E-03 |
| Bahrain | 0.909 | NA | NA | 2.955 | 0.478 | 16.162 | NA | 1.728E-04 | 2.793E-05 |
| Bangladesh | 14.469 | 62.820 | 9.089 | 33.378 | 0.925 | 2.770 | 1.183E-01 | 4.570E-01 | 1.266E-02 |
| Barbados | 14.651 | NA | NA | 14.043 | 1.148 | 8.174 | NA | 6.238E-04 | 5.099E-05 |
| Belarus | 43.195 | 156.100 | 67.427 | NA | NA | NA | 1.369E+00 | NA | NA |
| Belgium | 22.764 | NA | NA | 57.921 | 1.423 | 2.457 | NA | 1.776E-01 | 4.364E-03 |
| Belize | 55.986 | 211.000 | 118.131 | 85.845 | 1.469 | 1.712 | 2.695E-01 | 1.914E-01 | 3.277E-03 |
| Benin | 27.804 | 103.560 | 28.794 | 24.566 | 0.927 | 3.775 | 3.247E-01 | 2.852E-01 | 1.077E-02 |
| Bermuda | 20.000 | NA | NA | 20.308 | 1.468 | 7.226 | NA | 1.265E-04 | 9.143E-06 |
| Bhutan | 71.487 | 269.320 | 192.528 | 223.188 | 3.516 | 1.576 | 7.339E-01 | 9.009E-01 | 1.419E-02 |
| Bolivia | 46.925 | 131.260 | 61.594 | 66.840 | 0.945 | 1.414 | 6.672E+00 | 7.264E+00 | 1.027E-01 |
| Bosnia and Herzegovina | 42.733 | NA | NA | 97.419 | 1.826 | 1.874 | NA | 5.049E-01 | 9.462E-03 |
| Botswana | 26.917 | 155.250 | 41.789 | 4.301 | 0.688 | 15.988 | 2.368E+00 | 2.491E-01 | 3.982E-02 |
| Brazil | 59.417 | 171.920 | 102.151 | 90.008 | 1.283 | 1.426 | 8.538E+01 | 7.626E+01 | 1.087E+00 |
| British Indian Ocean Territory | NA | NA | NA | 44.928 | 10.494 | 23.357 | NA | 2.204E-04 | 5.148E-05 |
| British Virgin Islands | 24.133 | 210.000 | 50.680 | 36.103 | 3.368 | 9.330 | 7.602E-04 | 5.233E-04 | 4.882E-05 |
| Brunei | 72.106 | 247.000 | 178.102 | 218.515 | 6.617 | 3.028 | 9.386E-02 | 1.249E-01 | 3.783E-03 |
| Bulgaria | 35.860 | 180.500 | 64.728 | 65.432 | 1.444 | 2.208 | 7.027E-01 | 7.378E-01 | 1.629E-02 |
| Burkina Faso | 22.721 | 47.790 | 10.858 | 10.709 | 0.892 | 8.330 | 2.971E-01 | 2.921E-01 | 2.433E-02 |
| Burundi | 10.889 | 119.380 | 13.000 | 37.569 | 0.964 | 2.565 | 3.338E-02 | 9.375E-02 | 2.405E-03 |
| Cabo Verde | 11.345 | 95.000 | 10.778 | 37.244 | 2.419 | 6.494 | 4.343E-03 | 1.446E-02 | 9.392E-04 |
| Cambodia | 45.708 | 69.300 | 31.676 | 54.393 | 0.977 | 1.796 | 5.591E-01 | 9.848E-01 | 1.769E-02 |

| | | | | | | | | |
|---|---|---|---|---|---|---|---|---|
| Cameroon | 43.030 | 265.050 | 114.050 | 131.622 | 2.050 | 1.558 | 5.391E+00 | 6.111E+00 | 9.519E-02 |
| Canada | 38.151 | 90.430 | 34.500 | NA | NA | NA | 3.137E+01 | NA | NA |
| Cayman Islands | 53.000 | NA | NA | 5.400 | 0.922 | 17.071 | NA | 1.670E-04 | 2.851E-05 |
| Central African Republic | 35.801 | 217.090 | 77.719 | 82.979 | 1.061 | 1.278 | 4.842E+00 | 5.128E+00 | 6.555E-02 |
| Chad | 3.425 | 91.230 | 3.125 | 8.729 | 0.618 | 7.075 | 3.935E-01 | 1.105E+00 | 7.821E-02 |
| Chile | 24.492 | 219.270 | 53.704 | 52.282 | 0.986 | 1.887 | 3.993E+00 | 3.851E+00 | 7.266E-02 |
| China | 23.341 | 64.720 | 15.106 | 44.748 | 0.721 | 1.611 | 1.424E+01 | 4.195E+01 | 6.756E-01 |
| Clipperton Island | NA | NA | NA | NA | NA | NA | NA | NA | NA |
| Colombia | 53.305 | 184.130 | 98.151 | 124.083 | 1.837 | 1.481 | 1.089E+01 | 1.408E+01 | 2.085E-01 |
| Comoros | 17.699 | 66.000 | 11.681 | 80.896 | 2.202 | 2.722 | 2.173E-03 | 1.353E-02 | 3.683E-04 |
| Cook Islands | 64.958 | NA | NA | 142.774 | 13.583 | 9.514 | NA | 2.729E-03 | 2.596E-04 |
| Coral Sea Islands | NA | NA | NA | NA | NA | NA | NA | NA | NA |
| Costa Rica | 59.437 | 196.000 | 116.497 | 146.522 | 2.771 | 1.891 | 5.948E-01 | 7.494E-01 | 1.417E-02 |
| Croatia | 34.652 | 174.010 | 60.297 | 81.014 | 1.707 | 2.107 | 3.374E-01 | 4.462E-01 | 9.400E-03 |
| Cuba | 31.167 | 113.590 | 35.403 | 22.044 | 0.359 | 1.627 | 3.683E-01 | 2.423E-01 | 3.942E-03 |
| Curaçao | 0.158 | 79.000 | 0.125 | 5.080 | 0.648 | 12.753 | 5.530E-06 | 2.353E-04 | 3.001E-05 |
| Cyprus | 18.672 | 41.930 | 7.829 | 32.138 | 1.140 | 3.548 | 7.234E-03 | 1.734E-02 | 6.152E-04 |
| Czechia | 34.673 | 163.230 | 56.596 | 79.508 | 1.586 | 1.994 | 4.370E-01 | 6.262E-01 | 1.249E-02 |
| Democratic Republic of the Congo | 55.647 | 231.000 | 128.545 | 120.614 | 1.557 | 1.291 | 2.914E+01 | 2.786E+01 | 3.595E-01 |
| Denmark | 14.966 | 113.100 | 16.927 | NA | NA | NA | 7.108E-02 | NA | NA |
| Djibouti | 0.250 | 86.510 | 0.216 | 9.370 | 0.835 | 8.908 | 5.018E-04 | 2.047E-02 | 1.824E-03 |
| Dominica | 63.827 | NA | NA | 162.851 | 7.532 | 4.625 | NA | 1.189E-02 | 5.501E-04 |
| Dominican Republic | 44.382 | 82.700 | 36.704 | 56.468 | 0.988 | 1.749 | 1.773E-01 | 2.735E-01 | 4.784E-03 |
| East Timor | 61.944 | 150.000 | 92.915 | 125.799 | 6.915 | 5.497 | 1.382E-01 | 1.897E-01 | 1.043E-02 |
| Ecuador | 50.321 | 177.020 | 89.079 | 138.284 | 2.440 | 1.764 | 2.212E+00 | 3.526E+00 | 6.222E-02 |
| Egypt | 0.045 | 120.000 | 0.054 | 4.698 | 0.534 | 11.374 | 5.398E-03 | 4.704E-01 | 5.350E-02 |
| El Salvador | 28.180 | 113.610 | 32.015 | 52.067 | 1.000 | 1.920 | 6.633E-02 | 1.069E-01 | 2.054E-03 |
| Equatorial Guinea | 87.288 | 214.500 | 187.232 | 212.412 | 3.865 | 1.820 | 5.252E-01 | 5.665E-01 | 1.031E-02 |
| Eritrea | 10.448 | 72.520 | 7.577 | 15.293 | 1.019 | 6.661 | 7.653E-02 | 1.874E-01 | 1.248E-02 |
| Estonia | 56.094 | 115.870 | 64.996 | NA | NA | NA | 2.825E-01 | NA | NA |
| eSwatini | 28.928 | 76.050 | 22.000 | 22.187 | 1.036 | 4.671 | 3.784E-02 | 3.797E-02 | 1.773E-03 |
| Ethiopia | 15.244 | 121.310 | 18.492 | 27.053 | 0.786 | 2.904 | 2.071E+00 | 3.050E+00 | 8.857E-02 |
| Falkland Islands | 0.000 | 0.000 | 0.000 | 6.855 | 0.508 | 7.415 | 0.000E+00 | 7.950E-03 | 5.895E-04 |
| Faroe Islands | 0.057 | NA | NA | NA | NA | NA | NA | NA | NA |
| Federated States of Micronesia | 92.029 | NA | NA | 197.577 | 16.591 | 8.397 | NA | 1.252E-02 | 1.052E-03 |
| Fiji | 62.398 | 202.790 | 126.538 | 135.785 | 8.082 | 5.952 | 2.312E-01 | 2.570E-01 | 1.530E-02 |
| Finland | 73.736 | 59.770 | 44.072 | NA | NA | NA | 1.339E+00 | NA | NA |
| France | 31.509 | 135.500 | 42.695 | 63.643 | 1.308 | 2.055 | 2.338E+00 | 3.487E+00 | 7.164E-02 |
| French Guyana | 97.358 | 365.000 | 355.358 | 287.437 | 4.943 | 1.720 | 2.921E+00 | 2.391E+00 | 4.112E-02 |
| French Polynesia | 40.836 | 148.920 | 60.813 | 196.387 | 16.181 | 8.240 | 2.226E-02 | 6.552E-02 | 5.399E-03 |
| Gabon | 91.321 | 223.250 | 203.873 | 234.448 | 3.896 | 1.662 | 5.253E+00 | 6.095E+00 | 1.013E-01 |
| Gambia | 23.979 | 41.800 | 10.023 | 13.472 | 1.132 | 8.402 | 1.014E-02 | 1.415E-02 | 1.189E-03 |

| | | | | | | | | | |
|---|---|---|---|---|---|---|---|---|---|
| Georgia | 40.616 | 119.340 | 48.471 | 104.356 | 1.747 | 1.674 | 3.368E-01 | 7.260E-01 | 1.215E-02 |
| Germany | 32.732 | 185.140 | 60.601 | NA | NA | NA | 2.114E+00 | NA | NA |
| Ghana | 35.096 | 96.640 | 33.917 | 37.606 | 0.788 | 2.095 | 7.717E-01 | 8.975E-01 | 1.880E-02 |
| Gibraltar | 0.000 | 0.000 | 0.000 | 51.573 | 9.932 | 19.259 | 0.000E+00 | 1.904E-05 | 3.668E-06 |
| Greece | 30.270 | 34.240 | 10.364 | 51.351 | 1.263 | 2.460 | 1.336E-01 | 6.745E-01 | 1.659E-02 |
| Greenland | 0.001 | NA | NA | NA | NA | NA | NA | NA | NA |
| Grenada | 52.059 | 109.400 | 56.952 | 80.200 | 3.847 | 4.796 | 1.936E-03 | 2.785E-03 | 1.336E-04 |
| Guadeloupe | 42.556 | 347.000 | 147.670 | 69.759 | 2.336 | 3.348 | 2.496E-02 | 1.156E-02 | 3.871E-04 |
| Guatemala | 32.921 | 124.050 | 40.838 | 88.875 | 1.629 | 1.833 | 4.376E-01 | 9.671E-01 | 1.772E-02 |
| Guernsey | 5.250 | NA | NA | 38.197 | 6.862 | 17.965 | NA | 2.826E-04 | 5.077E-05 |
| Guinea | 25.187 | 131.190 | 33.043 | 52.373 | 0.847 | 1.616 | 8.119E-01 | 1.279E+00 | 2.068E-02 |
| Guinea-Bissau | 70.413 | 84.000 | 59.147 | 47.468 | 0.996 | 2.098 | 1.663E-01 | 1.558E-01 | 3.269E-03 |
| Guyana | 93.550 | 498.960 | 466.778 | 208.000 | 3.200 | 1.538 | 9.189E+00 | 4.393E+00 | 6.759E-02 |
| Haiti | 12.602 | 94.530 | 11.912 | 35.239 | 0.719 | 2.041 | 3.283E-02 | 9.476E-02 | 1.934E-03 |
| Heard Island and McDonald Islands | NA | NA | NA | NA | NA | NA | NA | NA | NA |
| Honduras | 56.835 | 105.720 | 60.086 | 106.327 | 1.909 | 1.795 | 6.723E-01 | 1.193E+00 | 2.142E-02 |
| Hong Kong S.A.R. | NA | NA | NA | 54.324 | 2.957 | 5.443 | NA | 5.629E-03 | 3.064E-04 |
| Hungary | 22.678 | 109.490 | 24.830 | 49.005 | 1.796 | 3.664 | 2.248E-01 | 4.567E-01 | 1.674E-02 |
| Iceland | 0.512 | 23.660 | 0.121 | NA | NA | NA | 1.215E-03 | NA | NA |
| India | 24.270 | 68.700 | 16.674 | 38.522 | 0.599 | 1.555 | 4.957E+00 | 1.214E+01 | 1.888E-01 |
| Indian Ocean Territories | NA | NA | NA | 172.175 | 8.879 | 5.157 | NA | 1.927E-03 | 9.938E-05 |
| Indonesia | 49.072 | 178.950 | 87.814 | 211.832 | 7.268 | 3.431 | 1.649E+01 | 3.982E+01 | 1.366E+00 |
| Iran | 6.601 | 137.670 | 9.088 | 15.166 | 0.798 | 5.261 | 1.480E+00 | 2.461E+00 | 1.295E-01 |
| Iraq | 1.900 | 51.110 | 0.971 | 3.700 | 0.518 | 13.996 | 4.217E-02 | 1.618E-01 | 2.265E-02 |
| Ireland | 11.352 | 111.640 | 12.673 | NA | NA | NA | 8.730E-02 | NA | NA |
| Isle of Man | 6.070 | NA | NA | NA | NA | NA | NA | NA | NA |
| Israel | 6.470 | NA | NA | 11.854 | 0.898 | 7.576 | NA | 2.596E-02 | 1.967E-03 |
| Italy | 32.522 | 110.600 | 35.970 | 64.779 | 1.247 | 1.925 | 1.058E+00 | 1.951E+00 | 3.756E-02 |
| Ivory Coast | 8.920 | 94.450 | 8.425 | 52.136 | 0.874 | 1.676 | 2.679E-01 | 1.672E+00 | 2.801E-02 |
| Jamaica | 55.114 | 158.500 | 87.356 | 86.060 | 1.539 | 1.789 | 9.461E-02 | 9.495E-02 | 1.698E-03 |
| Japan | 68.398 | NA | NA | 136.960 | 1.156 | 0.844 | NA | 5.116E+00 | 4.318E-02 |
| Jersey | 5.000 | NA | NA | 38.497 | 2.210 | 5.741 | NA | 4.583E-04 | 2.631E-05 |
| Jordan | 1.098 | 56.900 | 0.625 | 6.222 | 0.631 | 10.148 | 5.548E-03 | 5.529E-02 | 5.611E-03 |
| Kazakhstan | 1.280 | 82.470 | 1.055 | NA | NA | NA | 2.849E-01 | NA | NA |
| Kenya | 6.345 | 200.380 | 12.714 | 12.309 | 0.675 | 5.482 | 7.236E-01 | 7.159E-01 | 3.925E-02 |
| Kiribati | 1.457 | NA | NA | 20.593 | 2.918 | 14.171 | NA | 1.956E-03 | 2.772E-04 |
| Kosovo | NA | NA | NA | 54.639 | 2.040 | 3.734 | NA | 5.963E-02 | 2.226E-03 |
| Kuwait | 0.351 | NA | NA | 1.719 | 0.603 | 35.079 | NA | 3.004E-03 | 1.054E-03 |
| Kyrgyzstan | 6.858 | 49.660 | 3.406 | 40.009 | 2.316 | 5.789 | 6.532E-02 | 7.961E-01 | 4.608E-02 |
| Laos | 71.904 | 121.500 | 87.364 | 140.253 | 2.998 | 2.138 | 2.016E+00 | 3.199E+00 | 6.839E-02 |
| Latvia | 54.853 | 128.130 | 70.284 | NA | NA | NA | 4.370E-01 | NA | NA |
| Lebanon | 14.011 | 61.270 | 8.584 | 25.064 | 1.515 | 6.045 | 8.782E-03 | 2.506E-02 | 1.515E-03 |
| Lesotho | 1.137 | 73.720 | 0.838 | 19.730 | 1.315 | 6.667 | 2.545E-03 | 5.940E-02 | 3.960E-03 |

| | | | | | | | | | |
|---|---|---|---|---|---|---|---|---|---|
| Liberia | 79.085 | 205.400 | 162.440 | 149.037 | 2.353 | 1.579 | 1.565E+00 | 1.420E+00 | 2.242E-02 |
| Libya | 0.123 | 49.260 | 0.061 | 2.453 | 0.516 | 21.037 | 1.069E-02 | 3.984E-01 | 8.380E-02 |
| Liechtenstein | 41.875 | 242.410 | 101.509 | 85.524 | 11.487 | 13.432 | 1.624E-03 | 1.174E-03 | 1.577E-04 |
| Lithuania | 35.132 | 133.900 | 47.041 | NA | NA | NA | 2.947E-01 | NA | NA |
| Luxembourg | 36.502 | 180.700 | 65.959 | 88.124 | 2.384 | 2.706 | 1.603E-02 | 2.299E-02 | 6.220E-04 |
| Macao S.A.R | NA | NA | NA | 7.128 | 3.823 | 53.633 | NA | 2.144E-05 | 1.150E-05 |
| Macedonia | 39.710 | 71.640 | 28.448 | 61.028 | 1.461 | 2.393 | 7.175E-02 | 1.549E-01 | 3.708E-03 |
| Madagascar | 21.364 | 163.200 | 34.867 | 33.953 | 0.748 | 2.203 | 2.029E+00 | 2.013E+00 | 4.434E-02 |
| Malawi | 23.777 | 78.700 | 18.713 | 24.627 | 0.699 | 2.839 | 1.764E-01 | 2.405E-01 | 6.827E-03 |
| Malaysia | 58.177 | 209.870 | 122.096 | 174.140 | 3.370 | 1.935 | 4.011E+00 | 5.710E+00 | 1.105E-01 |
| Maldives | 2.733 | 135.000 | 3.690 | 9.979 | 6.600 | 66.139 | 1.107E-04 | 1.085E-04 | 7.177E-05 |
| Mali | 10.897 | 46.360 | 5.052 | 4.861 | 0.597 | 12.285 | 6.164E-01 | 6.089E-01 | 7.481E-02 |
| Malta | 1.438 | NA | NA | 26.903 | 2.805 | 10.428 | NA | 8.762E-04 | 9.137E-05 |
| Marshall Islands | 52.222 | 132.130 | 69.001 | 51.668 | 9.921 | 19.202 | 1.242E-03 | 8.516E-04 | 1.635E-04 |
| Martinique | 49.330 | 306.000 | 150.950 | 94.467 | 3.471 | 3.674 | 1.600E-02 | 1.037E-02 | 3.809E-04 |
| Mauritania | 0.303 | 53.110 | 0.161 | 1.734 | 0.520 | 29.965 | 1.661E-02 | 1.797E-01 | 5.386E-02 |
| Mauritius | 19.099 | 124.180 | 23.717 | 34.356 | 1.154 | 3.360 | 4.814E-03 | 6.921E-03 | 2.325E-04 |
| Mayotte | 37.541 | NA | NA | 70.923 | 2.571 | 3.626 | NA | 2.801E-03 | 1.015E-04 |
| Mexico | 33.793 | 52.440 | 17.721 | 43.643 | 0.578 | 1.323 | 3.445E+00 | 8.545E+00 | 1.131E-01 |
| Moldova | 11.755 | 93.360 | 10.974 | 30.794 | 2.026 | 6.578 | 3.608E-02 | 1.023E-01 | 6.726E-03 |
| Monaco | NA | 0.000 | NA | 70.127 | 8.049 | 11.478 | NaN | 1.321E-04 | 1.516E-05 |
| Mongolia | 9.123 | 54.900 | 5.008 | 9.351 | 0.604 | 6.463 | 7.781E-01 | 1.463E+00 | 9.457E-02 |
| Montenegro | 61.487 | 96.870 | 59.562 | 85.322 | 2.254 | 2.642 | 8.011E-02 | 1.171E-01 | 3.095E-03 |
| Montserrat | 25.000 | NA | NA | 50.760 | 9.031 | 17.791 | NA | 5.056E-04 | 8.994E-05 |
| Morocco | 12.867 | 39.890 | 5.133 | 8.757 | 0.624 | 7.131 | 2.291E-01 | 5.182E-01 | 3.695E-02 |
| Mozambique | 46.725 | 101.370 | 47.365 | 38.212 | 0.847 | 2.216 | 3.725E+00 | 2.986E+00 | 6.616E-02 |
| Myanmar | 43.707 | 125.540 | 54.869 | 128.739 | 2.213 | 1.719 | 3.583E+00 | 8.537E+00 | 1.468E-01 |
| Namibia | 8.064 | 67.400 | 5.435 | 6.383 | 0.671 | 10.511 | 4.475E-01 | 5.252E-01 | 5.520E-02 |
| Nauru | 0.000 | 0.000 | 0.000 | 28.300 | 6.009 | 21.233 | 0.000E+00 | 8.141E-05 | 1.729E-05 |
| Nepal | 41.591 | 172.230 | 71.632 | 133.964 | 2.540 | 1.896 | 1.027E+00 | 1.971E+00 | 3.736E-02 |
| Netherlands | 10.968 | 55.130 | 6.046 | NA | NA | NA | 2.037E-02 | NA | NA |
| New Caledonia | 45.844 | 146.000 | 66.932 | 87.037 | 5.975 | 6.865 | 1.224E-01 | 1.640E-01 | 1.126E-02 |
| New Zealand | 37.570 | 294.650 | 110.700 | 94.275 | 4.423 | 4.692 | 2.915E+00 | 2.531E+00 | 1.188E-01 |
| Nicaragua | 28.316 | 91.020 | 25.773 | 66.336 | 1.208 | 1.821 | 3.102E-01 | 8.537E-01 | 1.554E-02 |
| Niger | 0.852 | 38.200 | 0.326 | 2.156 | 0.538 | 24.942 | 4.124E-02 | 2.546E-01 | 6.352E-02 |
| Nigeria | 23.746 | 134.770 | 32.002 | 20.354 | 0.537 | 2.637 | 2.915E+00 | 1.847E+00 | 4.872E-02 |
| Niue | 72.577 | 112.050 | 81.322 | 97.162 | 12.186 | 12.542 | 2.114E-03 | 2.143E-03 | 2.688E-04 |
| Norfolk Island | 12.250 | NA | NA | 97.764 | 15.832 | 16.194 | NA | 4.023E-04 | 6.514E-05 |
| North Korea | 50.080 | 62.300 | 31.200 | 95.091 | 1.714 | 1.802 | 3.757E-01 | 1.164E+00 | 2.097E-02 |
| Northern Cyprus | NA | NA | NA | 9.742 | 0.839 | 8.612 | NA | 3.234E-03 | 2.785E-04 |
| Norway | 40.049 | 64.160 | 25.695 | NA | NA | NA | 7.815E-01 | NA | NA |
| Oman | 0.008 | 107.670 | 0.009 | 8.303 | 0.585 | 7.051 | 2.692E-04 | 2.584E-01 | 1.822E-02 |
| Pakistan | 4.833 | 75.300 | 3.639 | 24.932 | 1.190 | 4.772 | 2.806E-01 | 2.176E+00 | 1.039E-01 |

| | | | | | | | | |
|---|---|---|---|---|---|---|---|---|
| Palau | 90.022 | NA | NA | 109.849 | 12.123 | 11.036 | NA | 5.404E-03 | 5.964E-04 |
| Palestine | 1.684 | NA | NA | 12.120 | 1.058 | 8.726 | NA | 7.610E-03 | 6.641E-04 |
| Panama | 56.683 | 145.100 | 82.248 | 144.485 | 3.196 | 2.212 | 6.114E-01 | 1.077E+00 | 2.382E-02 |
| Papua New Guinea | 79.176 | 176.000 | 139.350 | 321.084 | 19.293 | 6.009 | 6.311E+00 | 1.494E+01 | 8.974E-01 |
| Paraguay | 40.529 | 69.860 | 28.314 | 7.747 | 0.187 | 2.416 | 1.125E+00 | 3.098E-01 | 7.486E-03 |
| Peru | 56.508 | 237.790 | 134.371 | 145.882 | 2.322 | 1.591 | 1.720E+01 | 1.882E+01 | 2.995E-01 |
| Philippines | 24.109 | 219.770 | 52.984 | 119.728 | 2.173 | 1.815 | 1.580E+00 | 3.511E+00 | 6.372E-02 |
| Pitcairn Islands | 70.000 | NA | NA | 37.336 | 3.762 | 10.077 | NA | 1.589E-04 | 1.602E-05 |
| Poland | 30.971 | 166.000 | 51.412 | NA | NA | NA | 1.574E+00 | NA | NA |
| Portugal | 36.153 | NA | NA | 37.360 | 1.441 | 3.857 | NA | 3.414E-01 | 1.317E-02 |
| Qatar | 0.000 | 0.000 | 0.000 | 2.020 | 0.495 | 24.523 | 0.000E+00 | 2.252E-03 | 5.524E-04 |
| Republic of Serbia | 31.130 | 156.990 | 48.871 | 73.449 | 1.913 | 2.604 | 4.274E-01 | 5.698E-01 | 1.484E-02 |
| Republic of the Congo | 64.264 | 198.800 | 127.756 | 142.063 | 2.186 | 1.538 | 4.363E+00 | 4.900E+00 | 7.538E-02 |
| Reunion | 39.219 | 125.000 | 49.024 | 67.755 | 2.625 | 3.874 | 1.230E-02 | 1.750E-02 | 6.779E-04 |
| Romania | 30.116 | 207.500 | 62.490 | 77.204 | 1.384 | 1.793 | 1.438E+00 | 1.825E+00 | 3.272E-02 |
| Russia | 49.784 | 77.330 | 38.498 | NA | NA | NA | 6.305E+01 | NA | NA |
| Rwanda | 11.188 | 146.060 | 16.341 | 38.381 | 1.287 | 3.353 | 4.031E-02 | 9.712E-02 | 3.257E-03 |
| Sáo Tomé and Principe | 54.063 | 162.500 | 87.852 | 216.015 | 6.190 | 2.866 | 8.434E-03 | 2.240E-02 | 6.420E-04 |
| Saint Barthelemy | 8.500 | 124.500 | 10.583 | 23.611 | 3.778 | 15.999 | 2.117E-05 | 5.766E-05 | 9.226E-06 |
| Saint Helena | 5.128 | NA | NA | 103.571 | 21.698 | 20.950 | NA | 3.797E-03 | 7.956E-04 |
| Saint Kitts and Nevis | 42.308 | 210.000 | 88.846 | 20.454 | 2.839 | 13.879 | 2.310E-03 | 5.402E-04 | 7.498E-05 |
| Saint Lucia | 34.049 | 294.020 | 100.111 | 121.243 | 6.501 | 5.362 | 6.107E-03 | 7.337E-03 | 3.934E-04 |
| Saint Martin | 24.800 | 124.500 | 30.876 | 30.793 | 4.463 | 14.493 | 1.544E-04 | 2.103E-04 | 3.047E-05 |
| Saint Pierre and Miquelon | 5.304 | 26.250 | 1.392 | 25.550 | 5.249 | 20.544 | 3.203E-05 | 6.203E-04 | 1.274E-04 |
| Saint Vincent and the Grenadines | 73.179 | 219.130 | 160.358 | 129.996 | 7.839 | 6.030 | 6.254E-03 | 4.780E-03 | 2.882E-04 |
| Samoa | 57.127 | 105.000 | 59.984 | 128.965 | 8.051 | 6.243 | 1.698E-02 | 3.586E-02 | 2.239E-03 |
| San Marino | 16.667 | 90.990 | 15.165 | 39.411 | 6.946 | 17.625 | 9.099E-05 | 2.377E-04 | 4.190E-05 |
| Saudi Arabia | 0.454 | 26.610 | 0.121 | 4.367 | 0.541 | 12.385 | 2.600E-02 | 8.391E-01 | 1.039E-01 |
| Scarborough Reef | NA | NA | NA | NA | NA | NA | NA | NA | NA |
| Senegal | 41.906 | 44.250 | 18.543 | 13.182 | 0.835 | 6.335 | 3.570E-01 | 2.587E-01 | 1.638E-02 |
| Serranilla Bank | NA | NA | NA | NA | NA | NA | NA | NA | NA |
| Seychelles | 73.261 | 172.810 | 126.602 | 53.716 | 3.410 | 6.349 | 5.824E-03 | 2.340E-03 | 1.486E-04 |
| Siachen Glacier | NA | NA | NA | 64.401 | 5.828 | 9.050 | NA | 1.345E-02 | 1.217E-03 |
| Sierra Leone | 35.119 | 82.000 | 28.797 | 58.199 | 1.075 | 1.846 | 2.079E-01 | 4.168E-01 | 7.696E-03 |
| Singapore | 21.930 | 135.710 | 29.761 | 33.098 | 2.566 | 7.753 | 2.113E-03 | 1.690E-03 | 1.310E-04 |
| Sint Maarten | 10.882 | NA | NA | 2.978 | 80.005 | 2686.430 | NA | 6.956E-06 | 1.869E-04 |
| Slovakia | 40.056 | 171.110 | 68.540 | 92.376 | 1.683 | 1.822 | 3.295E-01 | 4.476E-01 | 8.155E-03 |
| Slovenia | 61.461 | 253.100 | 155.558 | 138.997 | 2.470 | 1.777 | 3.133E-01 | 2.825E-01 | 5.020E-03 |
| Solomon Islands | 90.138 | 95.780 | 86.334 | 341.637 | 24.867 | 7.279 | 2.417E-01 | 9.292E-01 | 6.763E-02 |
| Somalia | 9.532 | 102.490 | 9.770 | 4.187 | 0.636 | 15.182 | 6.129E-01 | 1.976E-01 | 2.999E-02 |
| Somaliland | NA | NA | NA | 6.245 | 0.600 | 9.614 | NA | 1.045E-01 | 1.005E-02 |
| South Africa | 14.055 | 85.660 | 12.040 | 8.935 | 0.584 | 6.537 | 1.461E+00 | 1.090E+00 | 7.125E-02 |

| | | | | | | | | | |
|---|---|---|---|---|---|---|---|---|---|
| South Georgia and the Islands | NA | NA | NA | NA | NA | NA | NA | NA | NA |
| South Korea | 64.518 | 131.690 | 84.964 | 102.526 | 1.719 | 1.676 | 8.279E-01 | 1.010E+00 | 1.694E-02 |
| South Sudan | 11.329 | NA | NA | 25.612 | 0.681 | 2.657 | NA | 1.606E+00 | 4.266E-02 |
| Spain | 37.170 | 55.870 | 20.767 | 33.413 | 0.921 | 2.757 | 1.038E+00 | 1.694E+00 | 4.670E-02 |
| Spratly Islands | NA | NA | NA | NA | NA | NA | NA | NA | NA |
| Sri Lanka | 33.695 | 79.160 | 26.673 | 60.490 | 1.122 | 1.854 | 1.673E-01 | 4.010E-01 | 7.436E-03 |
| Sudan | 9.836 | 55.980 | 5.506 | 4.262 | 0.568 | 13.334 | 1.028E+00 | 7.918E-01 | 1.056E-01 |
| Suriname | 97.412 | 362.880 | 353.489 | 235.952 | 4.172 | 1.768 | 5.514E+00 | 3.424E+00 | 6.054E-02 |
| Sweden | 68.695 | 72.470 | 49.783 | NA | NA | NA | 2.028E+00 | NA | NA |
| Switzerland | 32.113 | 193.060 | 61.998 | 99.795 | 2.447 | 2.452 | 2.450E-01 | 4.135E-01 | 1.014E-02 |
| Syria | 2.843 | 49.980 | 1.421 | 3.341 | 0.536 | 16.054 | 2.609E-02 | 6.212E-02 | 9.974E-03 |
| Tajikistan | 3.054 | NA | NA | 47.861 | 2.904 | 6.068 | NA | 6.808E-01 | 4.131E-02 |
| Tanzania | 51.643 | 48.580 | 25.088 | 33.416 | 0.633 | 1.893 | 2.222E+00 | 2.981E+00 | 5.644E-02 |
| Thailand | 38.899 | 142.500 | 55.431 | 85.657 | 1.497 | 1.748 | 2.832E+00 | 4.407E+00 | 7.701E-02 |
| The Bahamas | 50.935 | 39.800 | 20.272 | 4.095 | 0.343 | 8.375 | 2.029E-02 | 5.156E-03 | 4.318E-04 |
| Togo | 22.233 | 120.950 | 26.891 | 27.539 | 0.722 | 2.623 | 1.463E-01 | 1.566E-01 | 4.108E-03 |
| Tonga | 12.431 | 194.440 | 24.170 | 68.249 | 7.022 | 10.289 | 1.740E-03 | 4.116E-03 | 4.235E-04 |
| Trinidad and Tobago | 44.481 | 90.170 | 40.109 | 138.748 | 2.795 | 2.014 | 2.058E-02 | 7.108E-02 | 1.432E-03 |
| Tunisia | 4.523 | 58.740 | 2.657 | 4.736 | 0.606 | 12.791 | 4.128E-02 | 7.418E-02 | 9.488E-03 |
| Turkey | 28.871 | 48.110 | 13.890 | 32.820 | 0.804 | 2.450 | 1.069E+00 | 2.560E+00 | 6.273E-02 |
| Turkmenistan | 8.782 | NA | NA | 3.715 | 0.575 | 15.480 | NA | 1.749E-01 | 2.708E-02 |
| Turks and Caicos Islands | 11.074 | 132.260 | 14.646 | 2.312 | 0.691 | 29.894 | 1.391E-03 | 1.029E-04 | 3.077E-05 |
| Tuvalu | 33.333 | NA | NA | 141.660 | 22.680 | 16.010 | NA | 3.261E-04 | 5.220E-05 |
| Uganda | 11.659 | 96.000 | 11.193 | 25.205 | 0.626 | 2.485 | 2.244E-01 | 5.290E-01 | 1.315E-02 |
| Ukraine | 16.727 | 140.000 | 23.418 | 40.680 | 1.039 | 2.554 | 1.357E+00 | 2.327E+00 | 5.943E-02 |
| United Arab Emirates | 4.468 | 74.430 | 3.325 | 4.974 | 0.642 | 12.910 | 2.362E-02 | 3.535E-02 | 4.564E-03 |
| United Kingdom | 13.186 | 115.000 | 15.163 | NA | NA | NA | 3.668E-01 | NA | NA |
| United States | 35.401 | 118.704 | 42.023 | 54.684 | 0.628 | 1.149 | 3.291E+01 | 4.273E+01 | 4.911E-01 |
| United States Minor Outlying Islands | NA | NA | NA | 5.933 | 2.094 | 35.290 | NA | 1.661E-05 | 5.863E-06 |
| Uruguay | 11.604 | 97.000 | 11.256 | 11.827 | 0.346 | 2.922 | 1.970E-01 | 2.097E-01 | 6.129E-03 |
| Uzbekistan | 8.673 | NA | NA | 5.700 | 0.589 | 10.332 | NA | 2.508E-01 | 2.591E-02 |
| Vanuatu | 36.284 | NA | NA | 147.054 | 9.525 | 6.478 | NA | 1.808E-01 | 1.171E-02 |
| Vatican | NA | 0.000 | NA | NA | NA | NA | NaN | NA | NA |
| Venezuela | 52.413 | 204.720 | 107.300 | 95.691 | 1.416 | 1.480 | 9.464E+00 | 8.734E+00 | 1.292E-01 |
| Vietnam | 47.225 | 62.710 | 29.615 | 93.824 | 1.794 | 1.912 | 9.183E-01 | 3.086E+00 | 5.900E-02 |
| Wallis and Futuna | 41.643 | 192.600 | 80.204 | 53.722 | 8.647 | 16.095 | 1.123E-03 | 7.485E-04 | 1.205E-04 |
| Western Sahara | 2.500 | 39.890 | 0.997 | 1.399 | 0.542 | 38.789 | 2.653E-02 | 1.266E-02 | 4.909E-03 |
| Yemen | 1.040 | NA | NA | 17.071 | 0.926 | 5.423 | NA | 7.734E-01 | 4.194E-02 |
| Zambia | 60.283 | 44.000 | 26.525 | 35.122 | 0.740 | 2.108 | 1.972E+00 | 2.634E+00 | 5.553E-02 |
| Zimbabwe | 45.094 | 94.980 | 42.830 | 15.974 | 0.957 | 5.994 | 1.657E+00 | 6.219E-01 | 3.728E-02 |